TEST-THEORY CORRELATION STUDY FOR AN ULTRA HIGH TEMPERATURE THRUST MAGNETIC BEARING

A Thesis

by

DESIREDDY VIJESH REDDY

Submitted to the Office of Graduate Studies of
Texas A&M University
in partial fulfillment of the requirements for the degree of

MASTER OF SCIENCE

December 2008

Major Subject: Mechanical Engineering

TEST-THEORY CORRELATION STUDY FOR AN ULTRA HIGH TEMPERATURE THRUST MAGNETIC BEARING

A Thesis

by

DESIREDDY VIJESH REDDY

Submitted to the Office of Graduate Studies of
Texas A&M University
in partial fulfillment of the requirements for the degree of

MASTER OF SCIENCE

Approved by:

Chair of Committee,	Alan B. Palazzolo
Committee Members,	Bryan P. Rasmussen
	Raktim Bhattacharya
Head of Department,	Dennis L. O'Neal

December 2008

Major Subject: Mechanical Engineering

ABSTRACT

Test-Theory Correlation Study for an Ultra High Temperature

Thrust Magnetic Bearing. (December 2008)

Vijesh Reddy Desireddy, B.E., Jawaharlal Nehru Technological University, India

Chair of Advisory Committee: Dr. Alan B. Palazzolo

Magnetic bearings have been researched by the National Aeronautics and Space Administration (NASA) for a very long time to be used in wide applications. This research was to assemble and test an axial thrust electromagnetic bearing, which can handle 1000 lb-f of axial thrust load, when rotating at high speed, in a high temperature environment of 1000 ^{0}F. This high temperature magnetic bearing system would be used in high performance, high speed and high temperature applications like space vehicles, jet engines and deep sea equipment.

An experimental procedure was developed to measure actual load capacity of the designed bearing in the test rig. All the results obtained from the experiment were compiled and analyzed to determine the relation between bearing force, applied current and temperature.

The thesis incorporates the assembly, testing of the electromagnetic bearing at various speeds and temperatures and compare predicted to measured force vs. speed, current, gap and temperature. The results showed that the high temperature thrust magnetic bearing is capable of handling 1000 lb-f at 1000^{0}F and 5500 rpm.

DEDICATION

To my family for their love, support and understanding.

ACKNOWLEDGMENTS

I would like to express my gratitude to Dr. Alan B. Palazzolo for giving me such a wonderful topic to research. He was a constant inspiration. His guidance and encouragement were invaluable towards the completion of this research. I would also like to thank Dr. Raktim Bhattacharya and Dr. Bryan Rasmussen for their knowledge and understanding.

Special thanks go to Mr. Randall Tucker for the solid model of the test rig concept and also for helping me throughout my research. I would like to thank all who shared time with me in the Vibration Control and Electromechanics Laboratory and for their patience and help. Thanks also go to my friends and the department faculty and staff for making my stay at Texas A&M University a memorable one.

TABLE OF CONTENTS

Page

CHAPTER Page

LIST OF FIGURES

Page

Page

Page

Page

LIST OF TABLES

Page

CHAPTER I

INTRODUCTION

1.1 Introduction

Magnetic bearings have brought about a new revolution in the field of rotary machinery because of their applications in extreme environment. Magnetic bearings use the principle of levitation because of which they have some unique properties such as absence of contact between rotating parts and active control of dynamic properties. As there is no contact between rotating parts in magnetic bearing, it eliminates the need for lubrication. This will allow engines to operate at speeds and temperature well beyond the limits of current technologies. These unique properties have made them a very reliable system even in extreme environment. Recent research has increased its application to the high temperature environment.

Magnetic bearings have very less bearing losses compared to the conventional bearings resulting in lower operating costs. Because of their lower maintenance costs and higher life span magnetic bearings are being implemented into turbo-machinery. In addition to supporting loads, magnetic bearings directly measure bearing reaction forces.

The objective of this research was to assemble the axial thrust bearing which will run at high rpm in high temperature environment, run tests at various speeds and temperatures and compare the results with the theoretical values.

This thesis follows the style and format of Journal of Mechanical Design.

1.2 Objectives

The objectives of the research are as follows:

- Assemble the Test Rig.
- Test the Magnetic bearing at various speeds, loads and temperatures.
- Compare predicted to measured force vs. speed, current, gap and temperature.
- Identify correction factors to compensate theory.

1.3 Literature Review

The idea of levitation of metal objects using magnetic bearing has been around since 1842[1]. Magnetic levitation bearing was successfully demonstrated around mid 1800's. But applications of permanent magnets exhibited problems when it was found that they were not able to levitate a body in all six directions. Permanent magnets could not exert enough magnetic forces for practical use [1]. Materials with diamagnetic properties were discovered in 1939, which would hover an object with stability using suitable permanent magnets. This led to more researchers getting interested in electromagnetic bearings.

Allaire et al [2] designed and tested a magnetic thrust bearing. It had a flat rotor disk and was designed to handle 187 N (42 lbf). There was no indication that the bearing could be operated in high temperature environment. Ohsawa et al [3] developed and tested a radial magnetic bearing capable of operating at 12,000 rpm at 399^{o}C. Mekhiche et al [4] tried to develop an 8 pole magnetic bearing to operate at 50,000 rpm and 593^{o}C (1100^{o}F), but reports show only room temperature results.

Harner et al [5] had research three soft magnetic materials for the thrust rotor disk. They are Aermet 100 Alloy, quenched and tempered AISI 4340 and Hiperco 27. AISI 4340 is considered for ambient temperature use. Aermet 100 alloy has ultra high strength, so it would be logical to use it for extreme loading condition. When saturation is a concern along with operation of thrust bearing at an elevated temperature, Hypreco 27 is the material to be used due to its high saturation flux density.

Mohiuddin [6] described and analyzed the working of a high speed and high temperature electromagnetic axial thrust bearing using handbook calculations and Ansys. He researched on the 3 shapes of thrust runners: uniformly thick, tapered and hyperbolic. His work suggests that hyperbolic shaped thrust runner with an inner diameter of 5.08cm and outer diameter of 13.71cm made of Hiperco 27 is the best possible option producing the least amount of stresses suitable to operate an axial thrust electromagnetic bearing at high rpm and high temperature environment.

Hossain [7] experimentally showed the results of a radial bearing that uses poles with permanent magnets, which was designed for supplying 500 lb-f at 1000°F. Provenza et al [8]. described the open loop, experimental force and power measurements of a radial, redundant-axis, magnetic bearing at temperatures of 1000 °F and rotor speeds to 15,000 rpm. Palazzolo and Kenny [9] of TAMU-VCEL described the single plane magnetic bearing with permanent magnet which has a lower coil resistance.

No paper was found showing the test results of thrust magnetic bearing at high temperatures. This thesis describes the operation of a ultra high temperature thrust

magnetic bearing, its test results and also its correlation with the predicted results when operated at 1000 ^{0}F, 5500 RPM and carrying 1000 lb-f.

1.4 Scope of Thesis

Chapter II provides information about an electromagnetic bearing. Heat treatment of the parts of the high temperature thrust magnetic bearing, forces and stresses induced along with the design of support bearings are described in this chapter.

Chapter III discusses the assembly of the ultra high temperature magnetic bearing. All the parts in the assembly are described followed by a step by step procedure for assembling the magnetic bearing.

Chapter IV presents the test results of the high temperature thrust magnetic bearing. It contains the tests results of force vs. speed, gap, current and temperature of the magnetic bearing.

Chapter V provides the calculated theoretical results and the correlation between the expected and tested results. The correlation is made at various speeds, gaps, currents and temperatures.

The summary of the correlation, conclusions of this research along with recommendations for future work are presented in chapter VI.

Appendix A describes the calibration of the load cell.

Appendix B contains the 2D drawings of the parts of the ultra high temperature thrust magnetic bearing.

1.5 Novel Contribution

The novel contributions and challenges of this project are followings:

- Operation of a "*High Temperature Thrust Magnetic Bearing*" at 1000 ^{0}F and high speed.
- Operation of a hyperbolic profile thrust magnetic bearing.

CHAPTER II

THEORY OF MAGNETIC BEARING TECHNOLOGY

2.1 Introduction

The idea of levitation of objects and applying magnetic force has been researched for more than a century. Levitation of rotating objects has brought a new revolution in the area of rotodynamics. The power density of any machine primarily depends on the peripheral speed at the location where the forces act. Many turbo machinery applications require high power density, for which high rotational speed, low weight and small volumes are required. Magnetic bearings have the capability to operate at high rotational speeds. Its weight and volume is much less compared to the equipment for fluid-film bearings.

The electromagnetic bearing system includes a mechanical system (rotor), an actuator, a sensor, and a controller providing the magnetic bearing system a certain degree of 'intelligence'. Therefore it is named as Active Magnetic Bearing (AMB). This bearing is an active element that enables accurate shaft positioning and integrates very easily into process control. The vibration of the rotor can also be actively damped.

2.2 Operation of Active Magnetic Bearing

Mohiuddin [6] describes the working of an Active Magnetic Bearing (AMB). The displacement of the supported rotor is measured by a sensor. A controller (e.g., a microprocessor) derives an appropriate control signal using the sensor information. The

control current is driven in the coil after the control signal is amplified by a power amplifier, causing a magnetic force to act on the rotor. The controller calculates the electromagnetic force in such a way that the rotor remains in this predefined and stable hovering position. A simple schematic of an electromagnetic bearing is shown in Figure 2.1.

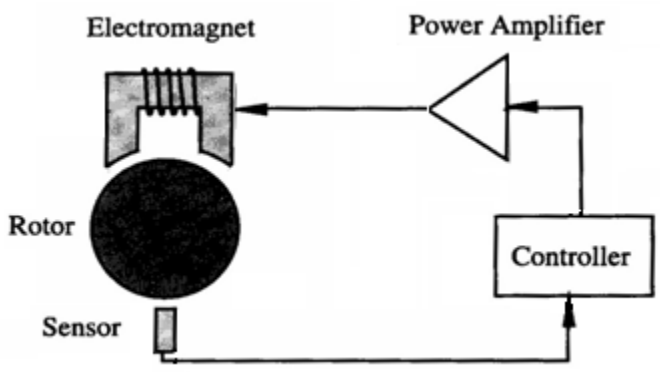

Figure 2.1 Active magnetic bearing system

The electromagnets are generally arranged in pairs of opposed coils for each degree of freedom in case of radial bearings. The coils are placed on the opposite side of the thrust disk for thrust bearings. A constant bias current energizes the coils to provide the dynamic control force.

2.3 Characteristics of Magnetic Bearing

Following are the most unique characteristics of a magnetic bearing. These characteristics allow them to be used in wide applications:

1. Magnetic bearings use the principle of levitation, so there is no contact between rotating parts. There is no lubrication, wear and tear and contamination.
2. The rotor can be rotated at high speeds, the strength of the material of the rotor being the only limitation.
3. Bearing losses in magnetic bearings are 5 to 20 times less than in conventional bearings at high operating speeds resulting in lower operating costs.
4. Lower maintenance cost and higher lifetime have to be expected due to the lack of mechanical wear. This is the main reason for the increasing application of magnetic bearing in turbo-machinery.
5. The dynamics of the contact-free hovering depends mainly on the implemented control law. Thus it is possible to adapt the stiffness and the damping, within physical limits, to the actual state of operation and the rotor speed.

There are always some drawbacks that go hand in hand with its characteristics. Few drawbacks involved with the magnetic bearing approach are:

1. The bearing is expensive due to its complexity.
2. The magnetic bearing technology is in rapid development, but for new users, a long-range assessment appears to be unclear.
3. Some aspects, such as reliability, safety, energy consumption or optimal design verifications are still in development.

2.4 Materials for Electromagnetic Bearings

Absence of mechanical wear and friction in the magnetic bearings make no theoretical limitation on the rotational speeds. The only limitation imposed on the rotational speeds is the material strength (stresses that it can withstand) of the rotor material in magnetic bearings. The prime concern in the design of magnetic bearings is the magnetic performance. Load capacity and power requirement of the magnetic bearings are greatly influenced by the material of the bearings. Power requirement and bearing load capacity also affects the material selection.

Mohiuddin [6] researched various materials for stator, rotor. His research showed that hiperco 50A was chosen as the material for the stator and hiperco 27 as the material for rotor. Inconel 718 was selected as the material for the high speed shaft. Its yield strength is 1035 MPa and thermal expansion of 13.0 μ.m/m.k.

2.5 Heat Treatment of Stator and Rotor Materials

The materials used in magnetic bearing are to be heat treated to some required temperatures to attenuate and retain their magnetic properties. Below are the heat treatment conditions for stator and rotor materials which are the 2 main parts:

(1) Two approximately 12 lb. solid rings (stators) of hiperco 50A material. The heat treat schedule for this material is:

- 1575/1600 ^{0}F for 2 to 4 hours in dry hydrogen and cool at 150/350 ^{0}F per hour until 600 ^{0}F is reached, after which any cooling rate can be employed.

(2) One approximately 10 lb. solid ring (rotor) of hiperco 27 material. The heat treat schedule for this material is the same as for (a).

2.6 Stresses in the Spinning Rotor Disk

Most of the axial thrust bearing assembly is made up of rotating parts. Therefore, dynamic loading induces a lot of stresses on those parts. According to the given design specification, the rotor disk operates at 30,000 rpm at 538^{o}C. When rotor spins centrifugal force acts upon it and attempts to pull it apart. The general trend of the stress distribution over the radius of a disk is shown in Figure 2.2. The maximum tangential stress appears at the inner radius of the disk. There is no radial stress at inner or outer radius of the disk. Radial stress is maximum at an interior point and is less than tangential stress at all other locations on the disc. The sum of tangential and radial stress is maximum at the inner radius of the disk. Rotational speeds of the rotor are proportional to the forces causing the stresses, because of which there will always be a constraint on maximum rotational speed for a rotor.

In the concept development stage, three shapes of rotor disk, uniformly thick, tapered and hyperbolic were chosen for the thrust bearing. The Roark's Formulas for Stress and Strain [10] has all the necessary equations for calculation of the stresses in the rotor disk.

From various plots & tables, Mohiuddin [6] calculated the radial and tangential stresses in the 3 rotor disks. It was clear that the hyperbolic shaped rotor disk diminishes the stresses by about 60% relative to the rectangular profile. This will enhance the capacity of the thrust runner to rotate at higher speed that usual thrust disk with same

inner and outer radius. Therefore, from the three concepts of thrust runner, the hyperbolic shaped rotor (Figure 2.3) was selected for the test rig.

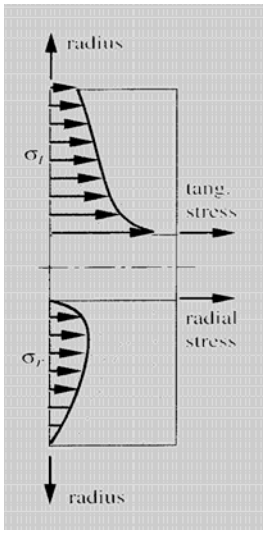

Figure 2.2 Stress distributions along the radius of a spinning rotor disk

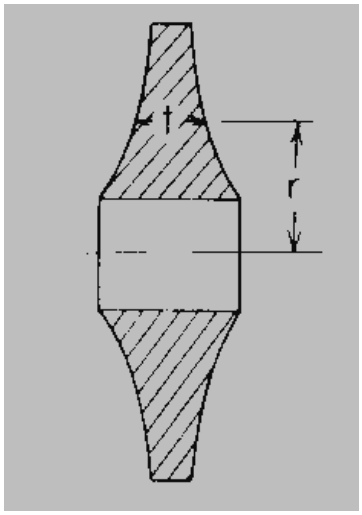

Figure 2.3 Hyperbolic shaped rotor disk

2.7 Effective Force Calculation

The profile of the rotor disk is decided to be hyperbolic. Apparently, it may be felt that the effective force on the disk may differ from that on a disk with flat profile.

Mohiuddin[6] calculated the forces on the disk of the 3 rotor disk profiles. From his results it was conclusive that force on the surface area of the disk is independent on the profile of the surface. The hyperbolic profile shall not only help to reduce the rotational stresses and weight of the disk but also make the set-up cost effective.

From the results generated from the handbook formulae Mohiuddin [6] decided that the only possible option open was to pick up the rotor with 5.08 cm of inner diameter made of Hiperco 27, which will be able to run fulfilling the required conditions.

2.8 Support Bearings

Electromagnetic bearings need some support incase of failure or overload. Support bearings are mainly selected based on its requirements i.e. what kind or load it needs to take, total load, direction of load. It also includes the basic characteristics of the machine in which it is to be used and also the big system.

Speed of the shaft has influence on the size of the support bearing. Operating environment with temperature, pressure and characteristics of working fluids have influence on the selection of support bearing. These factors also impose limitation on the lubricating fluid of the support bearing. Bearings should be preloaded as lightly as is necessary to achieve the desired results. This avoids excessive heat generation, which reduces speed capability and bearing life.

The support bearing was selected to be duplex pair angular contact bearing at each side of the rotor disk. It would be able to run at 31000 rpm and also able to take 14800 N thrust load. These duplex pair bearings were inside the bearing housing. On the other hand, a ring is attached to the containment vessel. The bearing housing would be attached to that ring by metal diaphragms. These diaphragms were stiff in radial direction and flexible in axial direction. The following Figure 2.4 shows the solid model of the support bearing module.

According to the design of the thrust bearing, the shaft will have 5.08 cm (2 in.) of diameter and it will rotate at 30,000 rpm. Barden Corporation catalog was followed to select the support bearing for the test set-up. The basic bearing nomenclature of the selected bearing is ZSB107J. It is an angular contact bearing with 3.5 cm (1.378 in.) diameter.

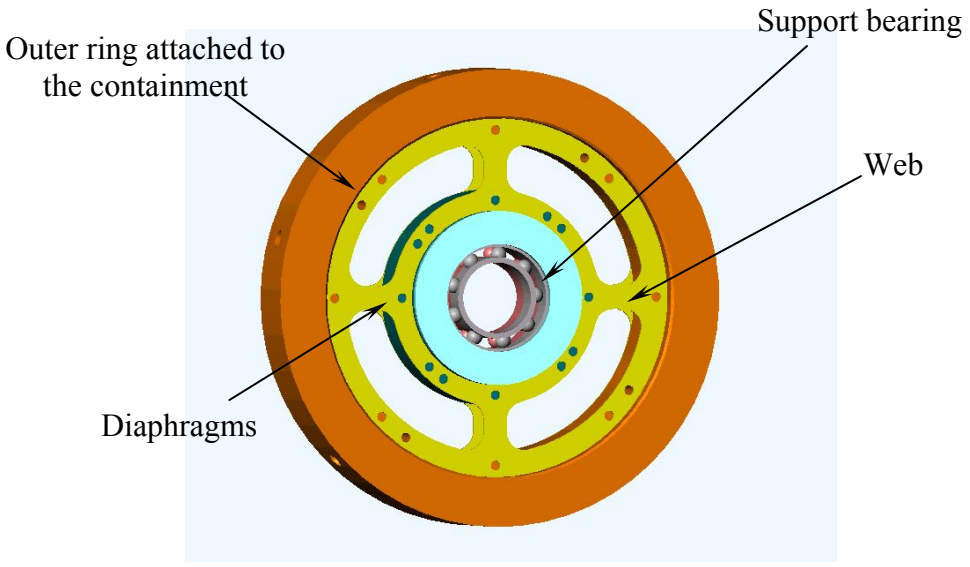

Figure 2.4 Radial support bearing module

CHAPTER III

ASSEMBLING OF TEST RIG

3.1 Parts of the Magnetic Bearing

There are lots of parts that go into the assembly of the Magnetic bearings. Each part has its own significance and contributes in the proper functioning of the whole machine. Figure 3.1 shows the outer safety cylinder with the support base. The assembly goes into this cylinder. The base is anchored to the ground to withstand the vibrations induced during the operation due to the high speeds.

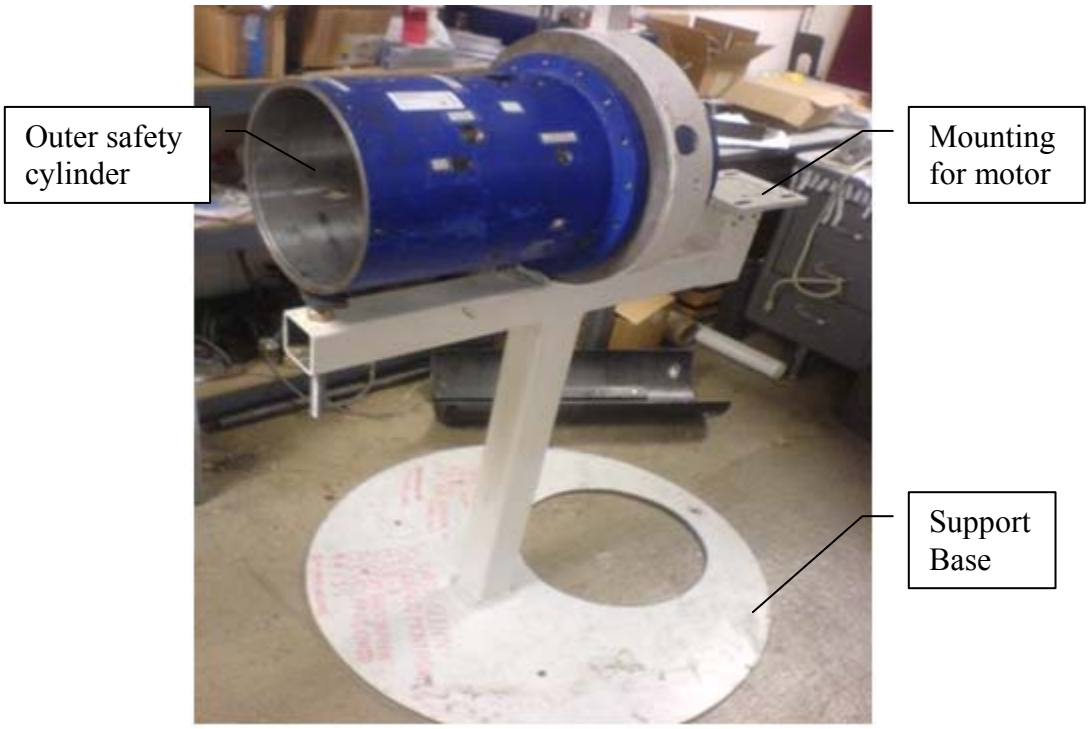

Figure 3.1 Outer safety cylinder with support base

Figure 3.2 shows the hyperbolic shaped rotor made of hiperco 27. Hyperbolic shaped rotor reduces stresses induced by 60% compared to a rectangular profile. The rotor does not have an interference fit with the shaft. It is held in its place by 2 sleeve's, one on each side.

Figure 3.2 Hyperbolic rotor

Figure 3.3 shows the stator made of hiperco 50A and a silver coil. There are 2 slots in the stator. 2 siver coils are placed in these slots and potted with high temperature ceramic and heat treated.

Figure 3.4 shows the high speed shaft. It is made of inconel 718 material. The shaft's front end has threads to mate with a motor. Cold air is blown into the shaft from the end to cool the bearings and the load cell.

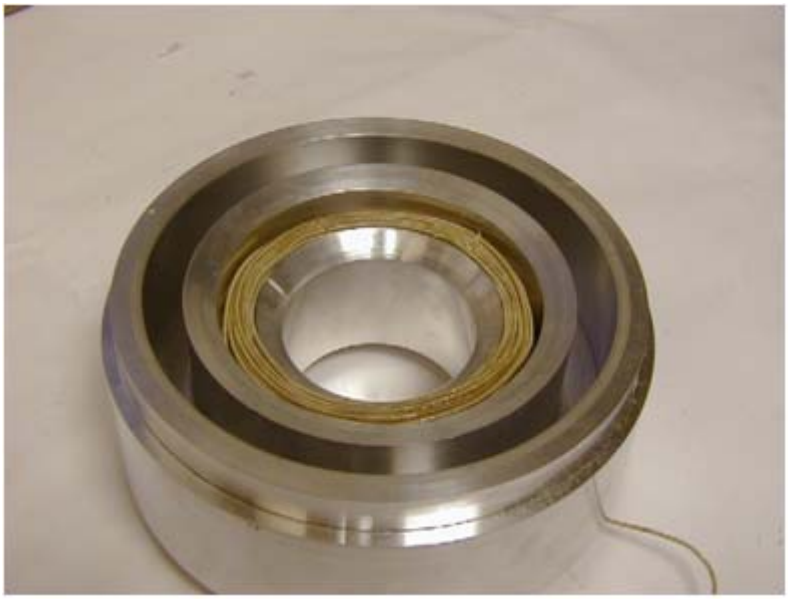

Figure 3.3 Stator with silver coil

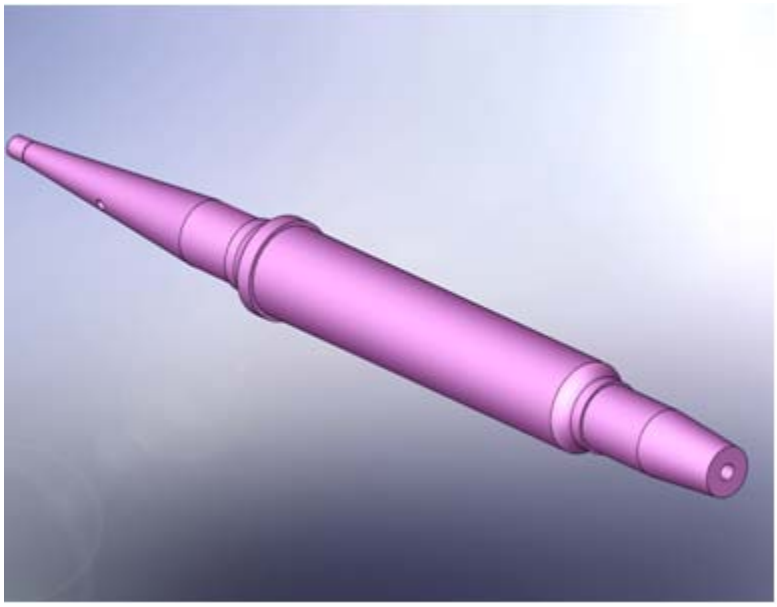

Figure 3.4 High speed shaft

The magnetic bearing is designed to operate at very high speeds, a powerful motor is required which can operate at 30000 rpm. This motor is fixed to an L-shaped frame, which is mounted on the base and fixed rigidly. The motor has a shaft coupling to mate with the shaft. Figure 3.5 shows the motor with its frame and coupling. The motor has to be aligned very carefully with the shaft so that there is threads mate perfectly. Even a small amount of misalignment can have a large effect on the efficiency of the entire system.

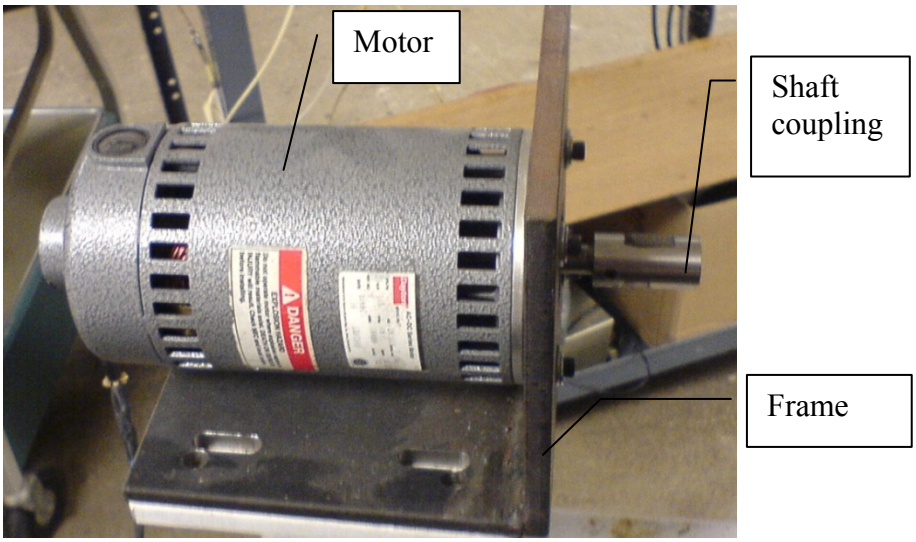

Figure 3.5 Motor with frame and shaft coupling

Figure 3.6 shows the balancing wheel. There are 2 balancing flywheels used in the assembly, one on each side of the rotor. Its main function is to provide balance to the rotor and to reduce the induced vibrations.

Figure 3.6 Balancing flywheel

Some of the main parts in the assembly are the shaft, stator, rotor, stator connector, sleeve, bearing housing. Figure 3.7 shows the first phase of the assembly with the above mentioned parts on it along with the cap screw assembly, which binds the 2 stators.

The swivel assembly connects the tension rods to the stator. Swivel assembly contains titanium heat stop foot socket, tension rods and screws. Figure 3.7 shows the swivel assembly, titanium heat stop foot socket (which acts as an insulation and prevents heat flow from stator to tension rods).

Insulation is required wherever possible to prevent heat from losing to the atmosphere. This helps in getting good performance evaluation of the whole system. Figure 3.8 shows a ceramic insulation which is placed over the stator. 4 pieces of insulation are placed on each stator.

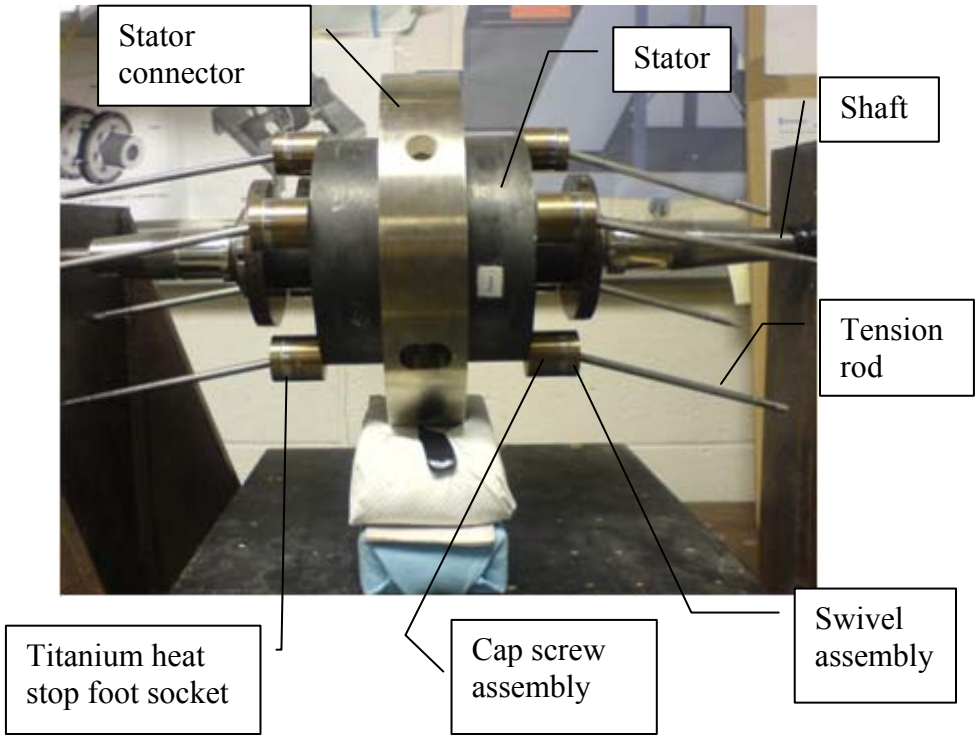

Figure 3.7 First assembly phase showing all main parts

Figure 3.8 Ceramic insualtion

There needs to be a gap between the stator and rotor inorder to have a magnetic flux to circulate. This gap is obtained by the metal shims (each 7 mils thick), which are placed between the stator and the stator housing. Figure 3.9 below, shows the metal shims. A total gap of 40 mils is maintained between rotor and stators.

Figure 3.9 Metal shims

There are 2 different sizes of shaft lock nuts used in the assembly. The bigger shaft lock nut is used as a collar to prevent the stator-rotor-sleeve-slywheel assembly from coming out. Smaller shaft lock nuts are used to hold the bearing housings in their places. Figure 3.10 shows a shaft lock nut.

Figure 3.10 Shaft lock nut

There are different shaft lock nut tighteneres for each size shaft lock nuts. Figure 3.11 and Figure 3.12 show lock nut tighteneres for big and small lock nuts respectively.

Figure 3.11 Lock nut tightener for big shaft lock nut

Figure 3.12 Lock nut tightener for small shaft lock nut

In order to achieve and maintain high temperatures for the operation of the magnetic bearing we need band heaters. Watlow band heaters are used for maintaining 1000 ^{0}F. These heaters require controllers which individually control the band heaters for each stator.

Another major part in the assembly is the bearing housing. This bearing housing contains the position ring, web, support bearings, bearing shoulder, copper tubes, ceramic tubes and a mating part for the force nut. Figure 3.13 shows the bearing housing. During operation the web takes the thrust forces and deforms. After the operation the web goes back to its initial position bringing back the rotor assembly back to its original position with the gap that was set initially. The 2 support bearings, one on each end of the magnetic bearing takes the weight of the magnetic bearing and balances it during operation. The copper tubes are used for pumping grease to the shoulder bearings at high temperature operations.

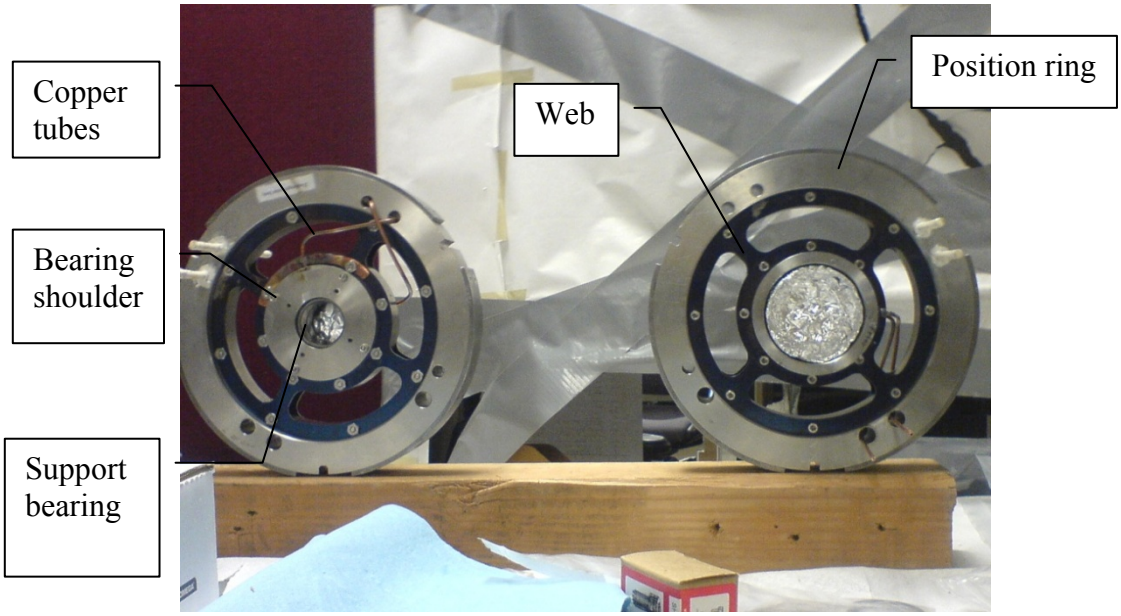

Figure 3.13 Bearing housing assembly

A force nut (Figure 3.14) is mounted on the bearing housing. There is a slot on the force nut to mount the load cell. Force nut is used for maintaining a preload on loadcell.

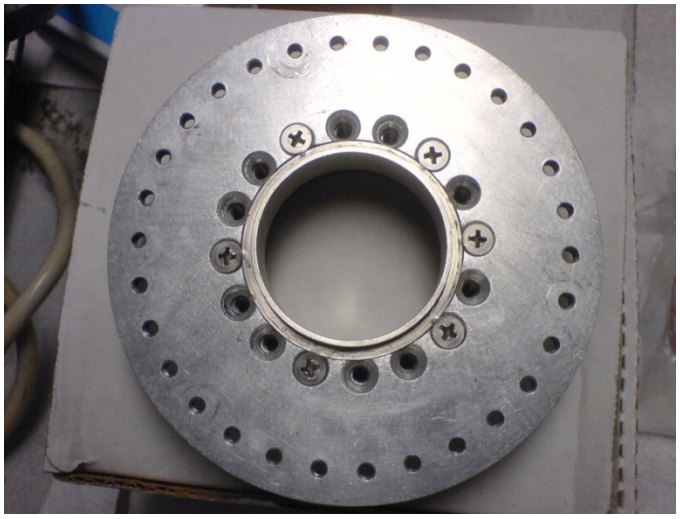

Figure 3.14 Force nut

There is a device bolted to the force nut to rotate it back and forth. This helps in adjusting the preload on the load cell, also prevents it from failure by keeping it within the safe overload limits during operation. Figure 3.15 shows the device for operating the force nut.

One of the most important devices in the assembly is the load cell. This is used to meaure the force generated by the magnetic field by reading the thrust force acting on it. The load cell used in the assembly can measure only compressive forces. Load cell specifications and caliberation is described in Appendix A. Figure 3.16 shows the load cell.

Figure 3.15 Device to operate force nut

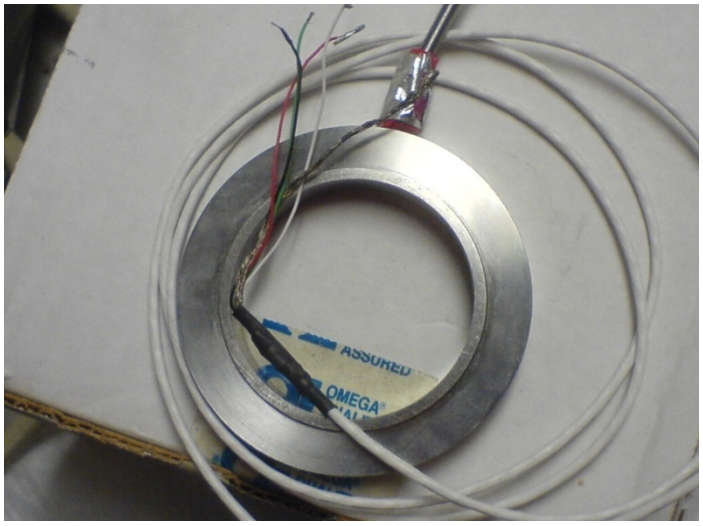

Figure 3.16 Load cell

An end cap is the part which holds the assembly to the outer safety cylinder. This has slot to mount the load cell. It also has holes for the tension rods, copper tubes, RTD wires, band heater wires, silvers wires. There is a set up for blowing cold air mounted on the back end outside the endcap. Figure 3.17 shows the end cap.

Figure 3.17 End cap

The end cap is fixed is to the outer safety cylinder using the end cap shoulder bolts (Figure 3.18). Shorter shoulder bolts (Figure 3.19) are used to hold the bearing housing to the outer safety cylinder.

Figure 3.18 End cap shoulder bolts

Figure 3.19 Shorter shoulder bolts

The stator radial positioning (SRP) bolts (Figure 3.20) position the stator such that there is a smooth rotation of the shaft. The beams are designed such that they take the

longitudinal forces acting on the SRP bolts. SRP bolt has slot at its bottom end where titanium foot for stator tilt adjustor is fixed using ceramic. This foot tilt adjustor adjusts the tilt of the stator and also prevents heat from escaping to the atmosphere. Figure 3.21 shows the custom made bolts for holding the SRP beams to the outer safety cylinder.

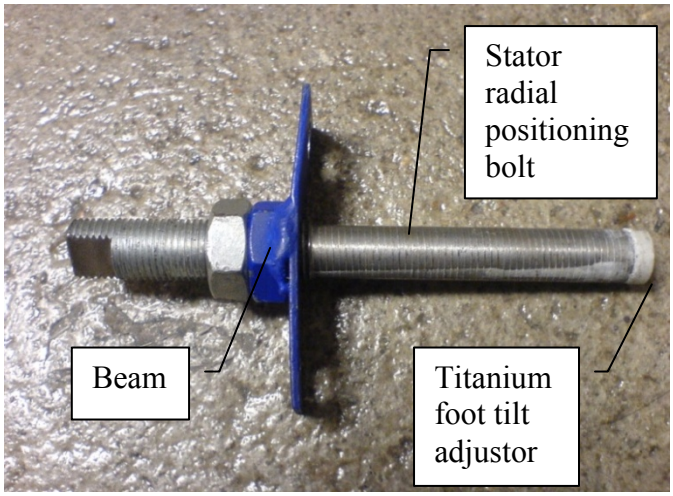

Figure 3.20 Stator radial positioning bolt

Figure 3.21 Custom made bolts for SRP beams

Figure 3.22 shows the mountings which are used to pump grease to support bearings. Axial positioning bolts are used to prevent the radial movement of magnetic bearing assembly. Figure 3.23 shows the axial positioning bolt along with the macor standoff stator connector.

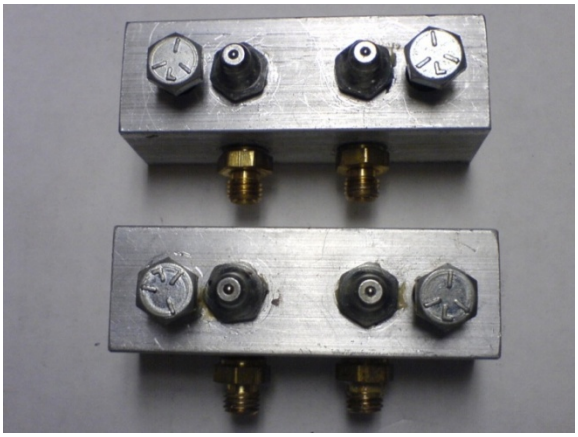

Figure 3.22 Mountings to pump grease to the catcher bearings

Figure 3.23 Axial positioning bolts with Macor standoff stator connector

There is a Bentley sensor (Figure 3.24) mounted at the front end of the shaft to measure the speed of the shaft. There are 2 RTD's placed on the stator with the silver coil. Their readings are taken using the RTD measuring device. Thermocouples are placed on each the bearing housings and also on the working load cell. Readings are taken regularly and care is taken the load cell is within safe operating temperatures.

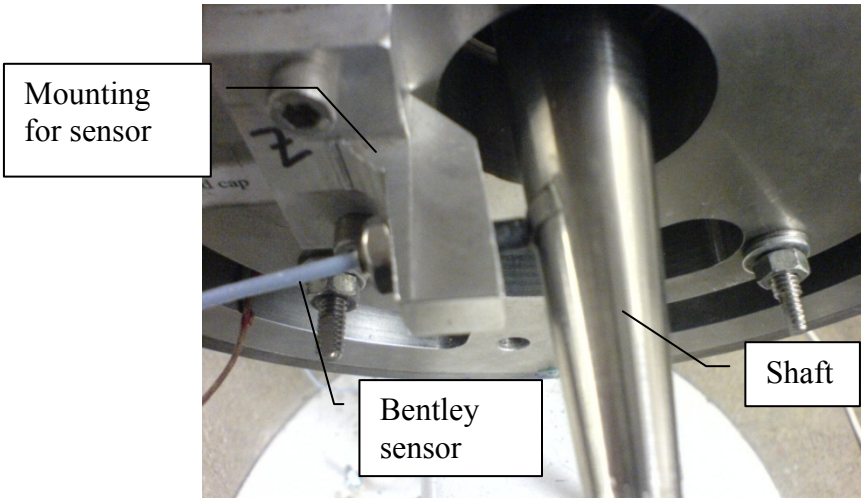

Figure 3.24 Bentley sensor and mounting

There are mountings at the back end of the magnetic bearing. One mounting is on the back of the shaft. This mounting is used for providing a passage for cold air and also to assist the position sensor to measure the movement of shaft. Figure 3.25 shows this shaft end mounting. Also, there is a mounting on the end cap at the end of the magnetic bearing. This mounting is used for holding position sensor and pipe which blows cold air. Figure 3.26 shows the mounting on the endcap.

Figure 3.25 Mounting on shaft

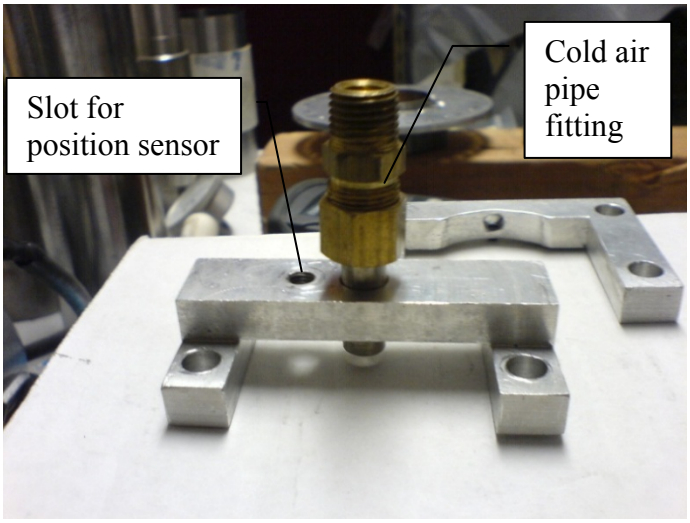

Figure 3.26 Mounting on end cap

During high temperature operations, it is important to keep the load cell within its safe operating temperatures. This is achieved by blowing cold air on it throughout the

operation. A nozzle (Figure 3.27) is specially made to mount on the side of the outer safety cylinder and blow cold air at the load cell.

Figure 3.27 Cool air blowing nozzle

3.2 Assembly

1. Take the shaft and clean it so that there are no dust particles or grease of any small amount on it. Use a clean cloth for doing this. Do not use a sand paper or any abrasive because it will tend to scratch the shaft. All the other parts are machined to fit the shaft with the required fits and tolerances no small amount of material has to be removed.
2. Take the balancing flywheel and clean the inside of it thoroughly. The shaft and the flywheel have an interference fit. So in order to fit the flywheel onto the shaft we need to cool the shaft and heat the flywheel. The shaft is cooled by placing it in a big bottle full of liquid nitrogen and leaving it for sometime. Since the liquid nitrogen

leaks out of the holes in the shaft, we need to place a tray below the bottle to collect the leaking liquid nitrogen. The important precaution we need to take when handling liquid nitrogen is that there is lot of ventilation and also that we do not leave it overnight in any enclosed place. We need to pour it out after using in the evening. The balancing flywheel is heated in the oven at 400^0c. The temperature in the oven is checked and maintained because over heating of the flywheel will damage its properties. After cooling the shaft for some time it is then taken and placed vertically on the hydraulic press. The flywheel is then taken and placed over the shaft very quickly before both of them come back to the room temperature. Using the press we apply some pressure on the flywheel and leave it for some time.

3. Take the left sleeve and clean it thoroughly. Since there is interference fit between the shaft and the sleeve the sleeve will not go on smoothly. Similar procedure as in step 2 is followed.
4. Left stator is cleaned and filed for any indentations and made to go over the shaft.
5. Rotor is then placed on the shaft. There is no interference with the shaft. Rotor goes and fits in the sleeve collar. Stator connector is then placed.
6. Right stator is cleaned and filed for any indentations and then made to go over the shaft.
7. Right balancing flywheel and right sleeve and are is placed using steps 2 and 3 respectively.
8. Shaft lock nut big is placed and tightened using the lock tightener.

9. Metal shims are placed between the stators and the stator connector to achieve 40 mils between stators and rotor overall.
10. Stators are held together by the cap screw assembly by passing the bolts through the stator, stator connector and then other stator and putting the nuts (one for tightening and one for locking). The nuts should be checked so that they are tight and maintain a uniform gap between the stator and rotor.
11. A metal protection is placed on the stator with the silver coil to protect the silver posts from getting damaged.
12. Watlow heaters are placed on each of the stators such that the nuts come onto the top. Figure 3.28 shows the heaters.

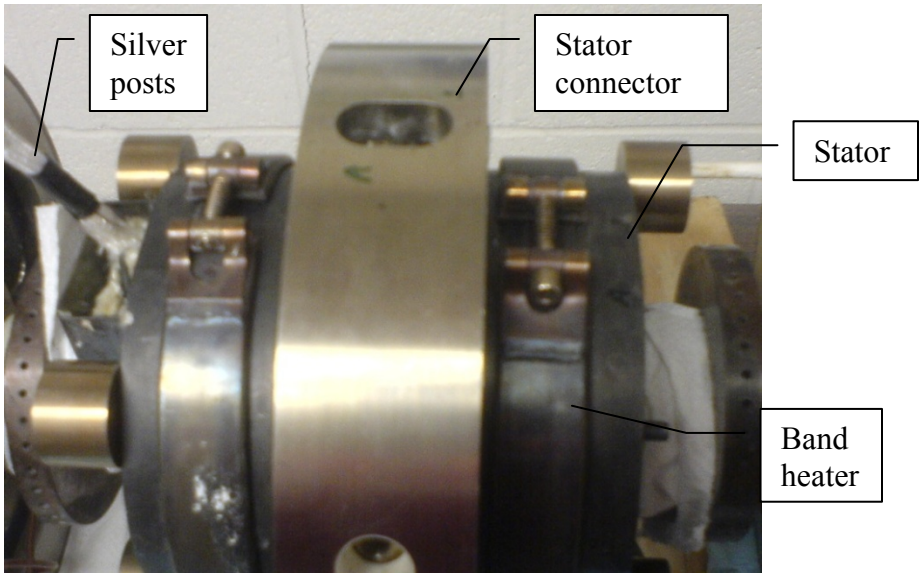

Figure 3.28 Assembly with band heaters, stator, stator connector and silver posts

13. The swivel assembly (titanium heat stop foot socket, tension rods, cap flange) are fixed to the cap screw assembly with bolts. These bolts are to be tightened very much so that they do not become loose when during operation (tightening and loosening of tension rods).
14. Step 13 is repeated on the other side of the shaft.
15. 2 RTD's are attached to the stator having the silver coil using the ceramic liquid.
16. Ceramic insulation is placed around the stator and held together by a metal ring. The 4 pieces of ceramic insulation are placed such that the piece which is different from all other 3 is placed on the top side of the stator so that it does not interfere with the protection for the silver posts.
17. Take the support bearings which are already assembled inside the bearing housing. Fix the bearing shoulder to the bearing housing with the bolts.
18. Take the position ring. Place the catcher bearing between the 2 webs and hold them using the bolts to the position ring.
19. Attach the copper tubes to the bearing housing so that they come outside.
20. Each of the bearing housing assemblies are placed on the shaft such that the bearing shoulder and the copper tubes face outside the assembly.
21. One shaft lock nut is placed on each side in the threading provided and tightened by the lock nut tightener so that the bearing housing assembly pushes against the collar of the shaft and does not move.

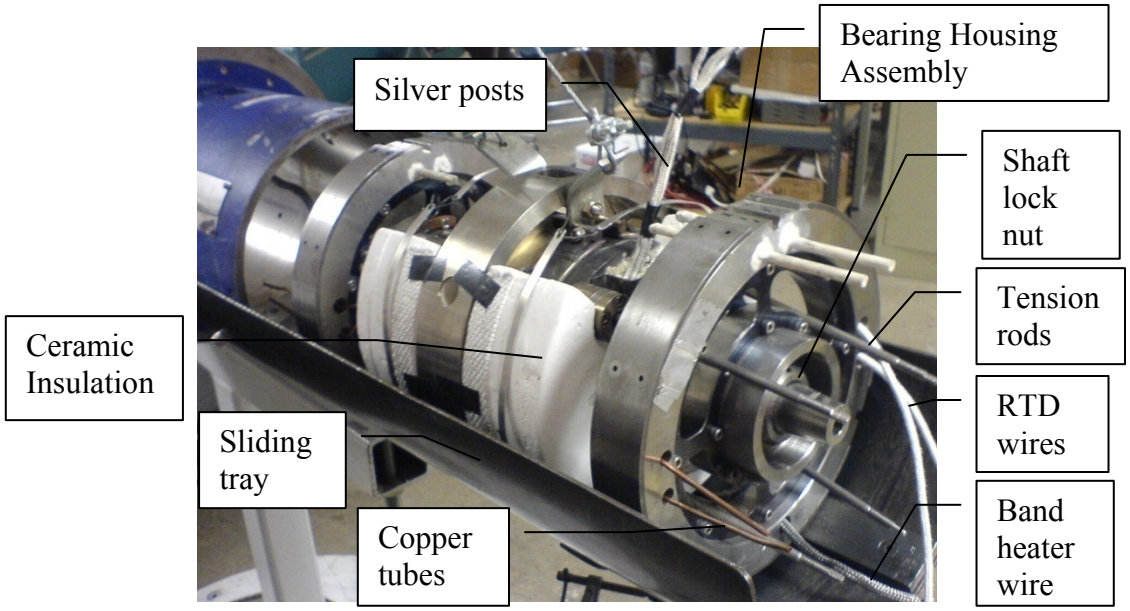

Figure 3.29 Assembly before being placed in outer safety cylinder

22. Force nut is mounted in the bearing shoulder using the threads of the shoulder. Same procedure is done on both bearing housings.
23. Thermocouple is mounted on the web of the bearing housing.
24. This whole assembly is placed inside the outside cylinder by using the stand and the sliding tray. Figure 3.29 shows the sliding tray.
25. Load cell is mounted on the force nut. Another thermocouple is mounted on the load cell to measure its temperature by using glue.
26. Figure 3.30 shows the end cap with all the wires. Silver wires come from the top 2 holes, heater wire comes from the bottom, RTD wires come from the side holes of

the end cap, thermocouple wire comes from the gap in the end cap, and copper tubes come from the left 2 holes.

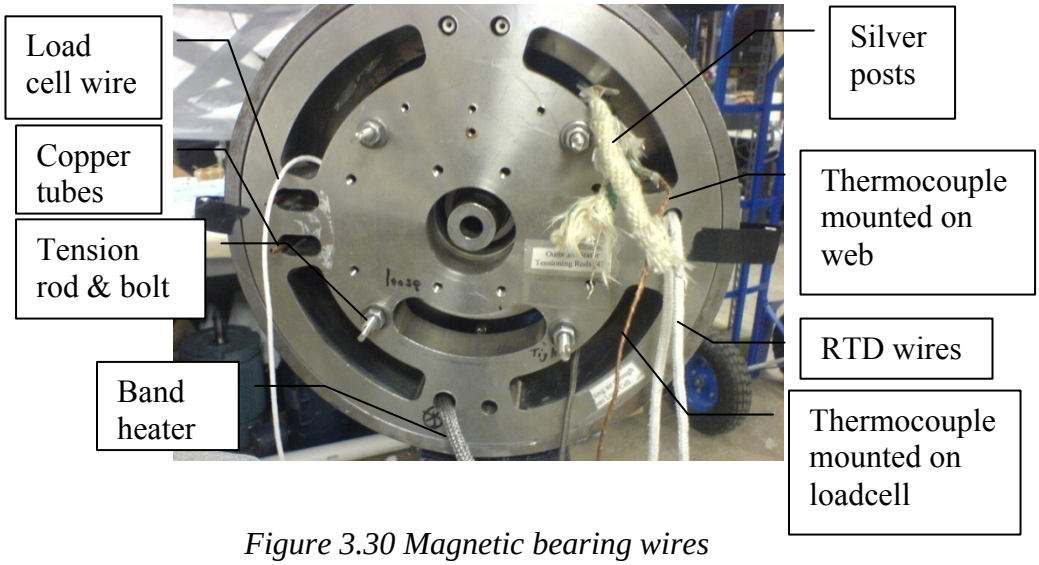

Figure 3.30 Magnetic bearing wires

27. Tension rods are made to pass through the holes in the end cap by using the hollow tubes. They are then tightened using the nuts.
28. Shoulder bolts are used to hold the end cap to the outer cylinder.
29. Shorter shoulder bolts are placed in their respective holes such that they hold the position ring and prevent it from rotating. These bolts are to be left loose until the actual testing.
30. Stator radial positioning bolts (Figure 3.31) are very unique for each hole. They are to be checked carefully such that they match the respective hole and beam. They are then placed in their respective holes and held using special bolts. Stator – rotor concentricity is aligned using these bolts.

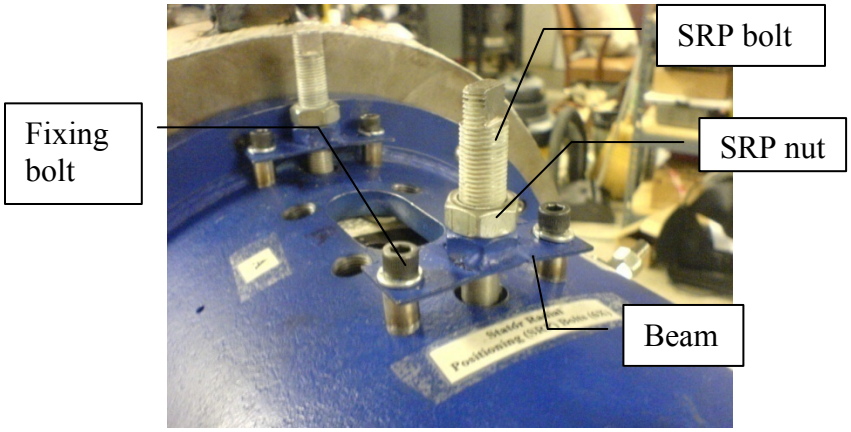

Figure 3.31 Stator radial positioning bolts

31. Axial positioning bolts along with the macor standoff stator connector (Figure 3.32) are to be placed in their respective holes to prevent the stator connector from rotating.

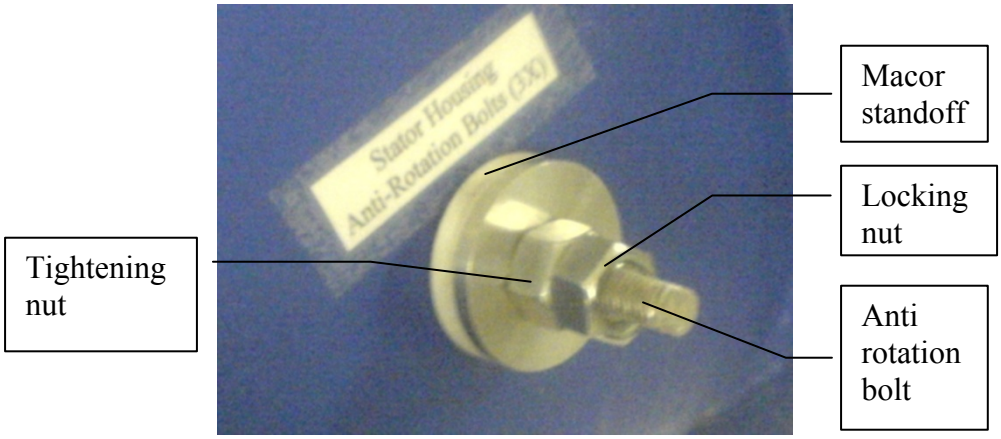

Figure 3.32 Axial positioning bolts

32. Motor with the coupling for shaft are placed on the mounting of the base. The bolts holding the outer cylinder and base are adjusted so that the coupling slides onto the shaft and the threads mate perfectly. This is done as to reduce the friction being generated (due to uneven mating) and thereby reduce the power required by the motor. Figure 3.33 shows the motor with the shaft coupling.

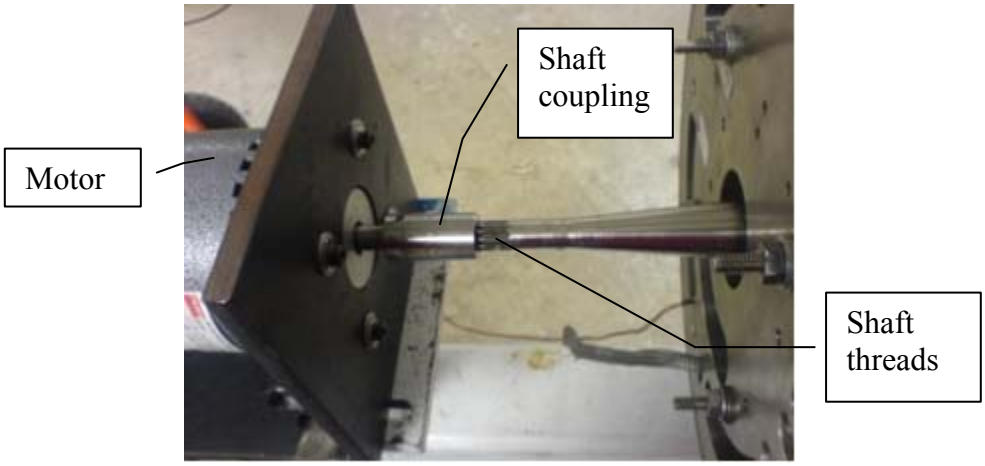

Figure 3.33 Motor with shaft coupling

33. Mounting for the bentley sensor are placed on the front side of the end cap such that it reads the speed of the shaft. There should be a gap of 30 mils between the tip of the sensor and the metal shim on the shaft to get voltage difference to get effective measurement. Figure 3.34 shows the senor and its mounting.

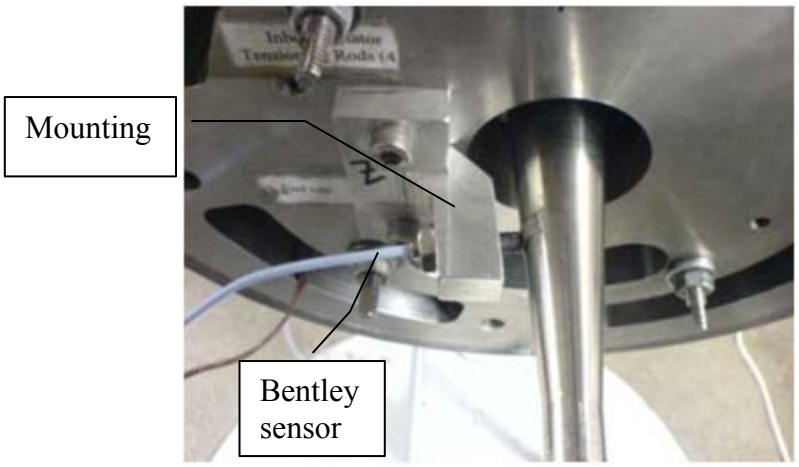

Figure 3.34 Bentley sensor and mounting

34. Cool air blowing nozzles are bolted on the on the outer cylinder. The cup end of the nozzle points towards the catcher bearings. This is done to remove the heat off the bearings and prevent them from seizing during the high temperature operations.
35. Separate mountings are done at the back of the shaft so as to blow the cold air through the shaft. Connections are made from this mounting to the cold air blowing nozzles on the side, to blow cold air on the load cell directly and prevent it from going over its temperature ranges.

3.3 Magnetic Bearing Assembly Explanation

The HTTMB test rig utilizes a rotor that is held in the radial direction by sliding bearing housings. This enables the shaft to translate axially and the rolling element bearings that support the shaft in the radial directions. The rotor assembly is shown in

Figure 3.35. The shaft bearing housings are restrained from rotating with the shaft by three bolts on each end that extend into axial slots outer bearing housing.

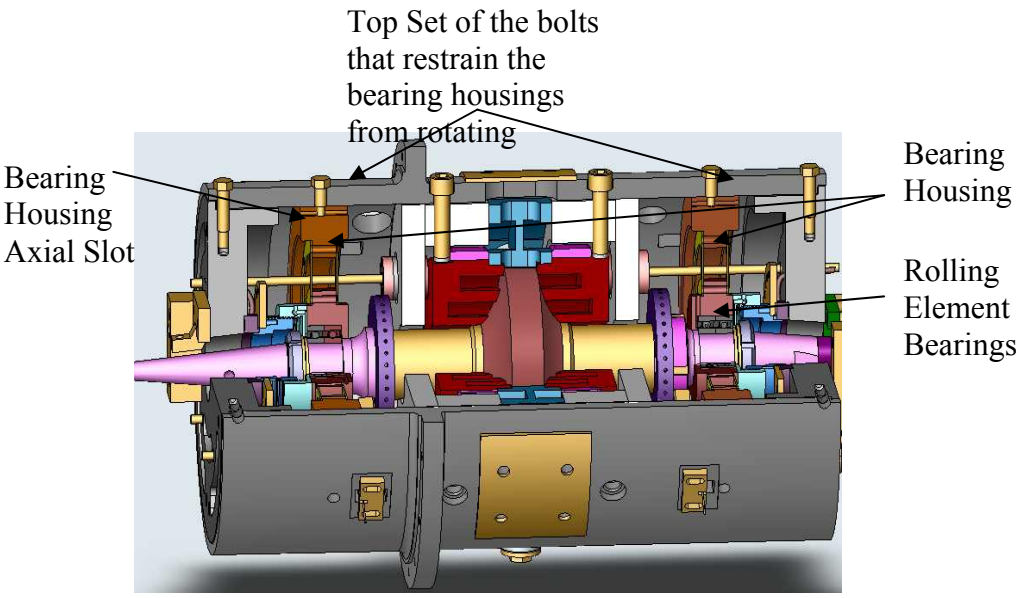

Figure 3.35 The HTTMB test rig showing the axial slots in the rotor bearing housing.

The electromagnets in the stator assembly are supported in the radial direction by the six stator support bolts and beams that are shown in Figure 3.36 and in the axial direction by the eight tension rods. The stator rotation is prevented by the three anti-rotation bolts. These bolts extend into the stator connection ring and will connect the housing to the connection ring and apply a slight tension. This allows the cold or hot system to be adjusted to compensate for the great temperature changes that the test rig operates through.

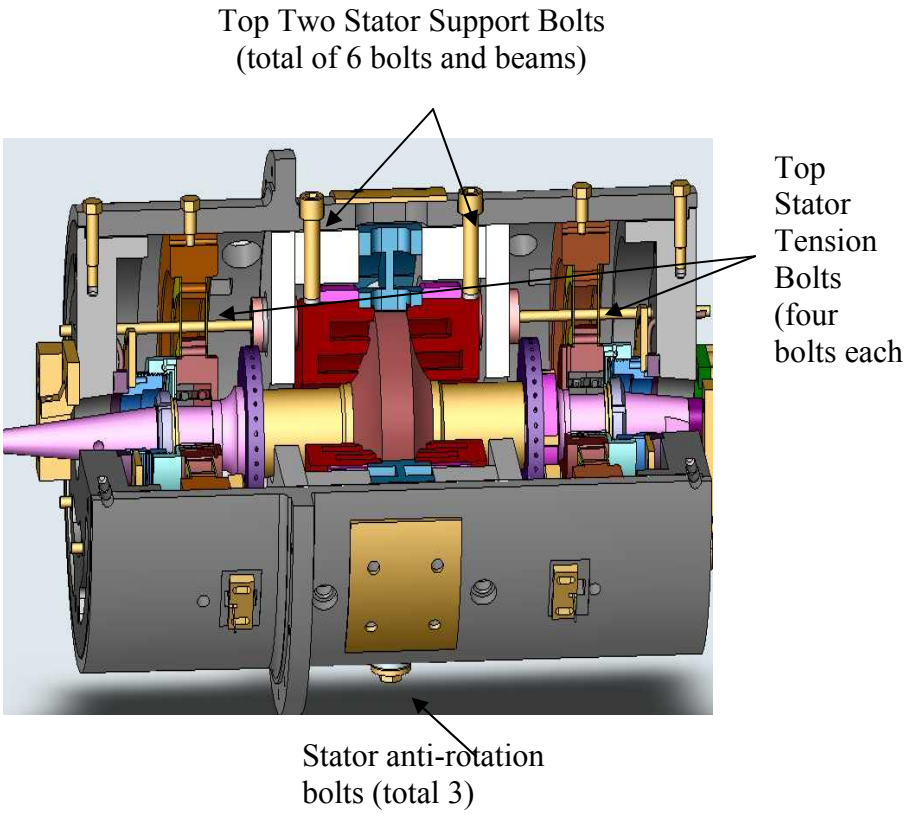

Figure 3.36 Test rig showing stator support bolts, tension rods and anti-rotation bolts

There are three port covers that are used to protect experimenters while the system is rotating at high speed. The port windows below the covers are used in the alignment and shaft location process. These port windows are labeled A, B, C. Measurements can be taken of the distance of the rotor disk to the stator connector outside to compare with the other port rotor and stator connector outer readings to determine the rotor stator concentricity. The tool used to measure the distance is shown in Figure 3.37 and is named the stator radial positioning tool (SCMT) (concentricity measurement). The gap between the rotor and the stator is measured with standard metal feeler gauges.

Figure 3.37 The stator radial positioning tool

Whenever the stator is to be realigned for concentricity the top two stator support bolts should be loosened and then the bottom two sets of bolts adjusted to bring the stator to the desired position. Loosen and tighten both bolts on B or C as necessary to obtain the same readings at all three locations, A, B, C. After locating the stator, tighten bolts are tightened at A and a final concentricity check is done.

The stator tension bolts must be retightened after heating and loosened after testing and before cooling to prevent breakage of the ceramic disks. By rotating each tension bolt on the outboard end approximately ¼ turn equally will usually suffice to temperatures of about 650^0F. Higher temperatures may take more. All rods must be tightened equally and this can be checked by attempting to push the tension rods from side to side. When it becomes too difficult to move the rods from side to side with your fingers the tensions are ok.

A load cell that is in between the outer end cap and the rotor axial position nut reads the force supplied by the rotor stator. A thumbwheel is attached to the nut and can be rotated to cause the distance to change along the shaft. Shown in Figure 3.38 is the thumbwheel slot and the locking device.

Figure 3.38 The thumbwheel slot and locking device

The total gap set in the rotor and stator assembly is 40 mil and by using a chain vice grip on the shaft with a protective brass shim the shaft can be pulled in and outboard to determine the shaft travel. If the shaft travel is less than 36 mils, the stator concentricity and the tension rods need to be adjusted. Once the rotor travel is correct the motor is then installed using the coupling alignment tools or by shimming the motor in such a way that will allow the coupling to slide backwards and forwards along the length of the shaft. When the coupling slides smoothly the shaft is aligned fairly well. When the shaft is aligned properly the shaft coupling will remain cool during operation.

3.4 Magnetic Bearing Operating Parameters

Some of the operating parameters that to be followed are given below:

1. Must loosen the bearing housing bolts when setting the load cell
2. Must have ~ 493 reading on A, B and C with special Dial Indicator Tool, at 500° F Stator temperature. Figure 3.39 shows the ports in the stator connector.

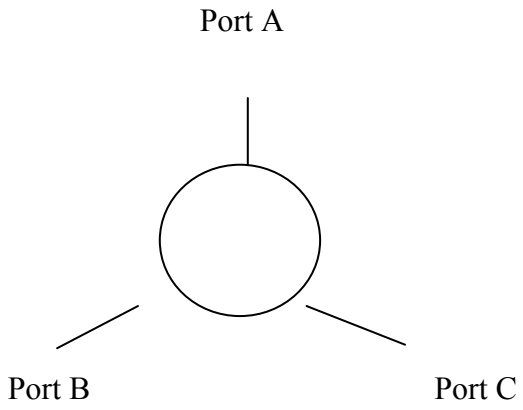

Figure 3.39 Viewed standing outboard looking inboard

3. Tap outboard bearing housing in axial direction with small piece of wood and rubber mallet. This is a necessary "assist" when rotating thumb wheel to advance outboard load cell inwards. Set Load Cell @ -1.5 mv preload prior to applying magnetic force.
4. When 1000 lbs. is applied check A, B, C gaps with feeler gages inserted in ports A, B and C. Each should be ~ 11. Mils and the current should be ~ 12 A at 500 ° F.
5. When all else it set up move the inboard dummy load cell inwards so that if the shaft is pulled inwards there still is a 10-15 mil gap after the shaft hits the dummy load cell (This will protect the inboard stator).
6. Continuously monitor load cell temp. and maintain it below 140 ^{0}F with cold air.
7. Gently separate outboard stator temp RTD wires through outboard balance port if RTD display blanks.
8. Only tighten bearing housings just prior spinning the rotor at high speeds. The housing must slide during axial alignment of the stator and during temperature transients.

CHAPTER IV

TESTING AND RESULTS

4.1 Experimental Test Setup

Assembling procedure is explained in detail in chapter III. After assembling the magnetic bearing, the next main thing is connect all the wires to their respective instruments. Power supply wires are connected to the silver wires coming out of the stator. There are 2 silver wires coming out from each loop in the stator. One combination of wires from each loop combines their respective magnetic fields and other combination cancel each other's field. This combination is found out by connecting one wire from each loop to the power supply and checking the magnetic force. The combination which has a great increase in magnetic force at high currents is the correct combination. RTD wires have to be connected to the RTD measuring gauge. A bentley sensor is connected to a Bentley sensing gauge, which is connected to a digital tachometer. Thermocouple wires are connected to the thermocouple gauges which are connected to multimeters. 2 wires (red and black) of the load cell are connected to the output voltmeter and other 2 wires (white and green) are connected to the input voltmeter. Watlow band heaters are connected to watlow band heater controllers. There are pipe fittings at the back and side of the assembly to blow cold air, to keep load cell within its safe operating temperatures. A duct is provided on the top for hot gases to be pumped out using a motor. Figure 4.1 shows the test set up of the magnetic bearing.

Figure 4.1 Test set up

4.2 Tests and Results at Room Temperature and 0 rpm

The magnetic bearing is first tested at room temperature (75 ^{0}F) and 0 rpm. For this test the voltmeter and power supply are switched on. 10 Vdc voltage is supplied to the load cell. The current was varied from 0 to 13A. Table 4.1 and Figure 4.2 show 2 test results for gap of 25 mils between the rotor and the stator with the silver coil. At 0 A the load cell is preloaded to 47.1 lbs force. These results show that a 1000 lb-f is obtained at 12 A.

Table 4.1 Force vs current at room temp, 0 rpm, gap of 20, 25 mils

	Tested Force (Lbs), 25 mils gap	
Current (A)	**Test 1**	**Test 2**
0	47.1	47.1
1	49	49.1
2	57.8	62.58
3	85.1	100.01
4	135.33	160.39
5	201.6	224.24
6	277	295.32
7	365.2	373.94
8	482.62	466.1
9	618	598.65
10	770.9	746.23
11	895.53	883.12
12	994.1	1005.27
13	1080.2	1086.41

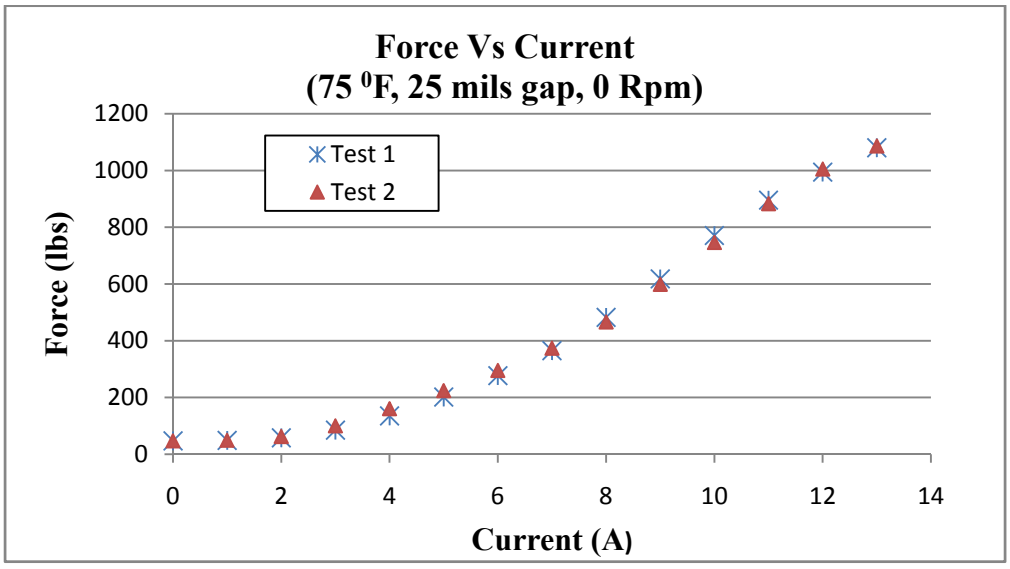

Figure 4.2 Force vs current at room temp, 0 rpm, gap 25 mils

Table 4.2 and Figure 4.3 show the forces for gaps of 20 mils and 25 mils between the rotor and the stator with the silver coil. The current was varied from 0 to 13A and temperature is 75 ^{0}F. At 0 A the load cell is preloaded to 47.1 lbs force.

Table 4.2 Force vs current at room temp, 0 rpm, gap of 20, 25 mils

	Tested Force (Lbs)	
Current (A)	**Gap 20 mils**	**Gap 25 mils**
0	47.1	47.1
1	49	49
2	60.6	57.8
3	104.9	85.1
4	171.8	135.33
5	254.34	201.6
6	348.54	277
7	461.6	365.2
8	613	482.62
9	778.7	618
10	915.3	770.9
11	1018	895.53
12	1109.7	994.1
13	1199.5	1080.2

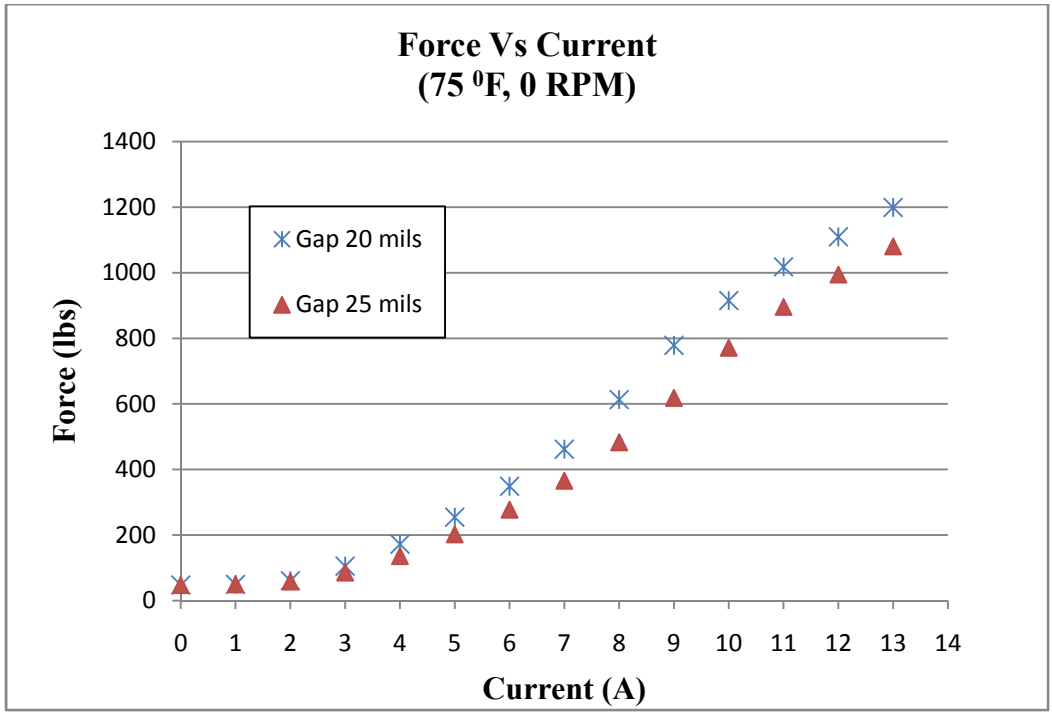

Figure 4.3 Force vs current at room temp, 0 rpm, gap 20 and 25 mils

4.3 Tests and Results at Room Temperature and High Speeds

Next stage of testing of magnetic bearing is at high speeds. For high speeds operation a shield was designed and placed on the test rig. This was done to prevent scrap and loose parts from flying off and injuring. Figure 4.4 shows the set up with the shield. Metal covers are placed at the front and back end of the bearing.

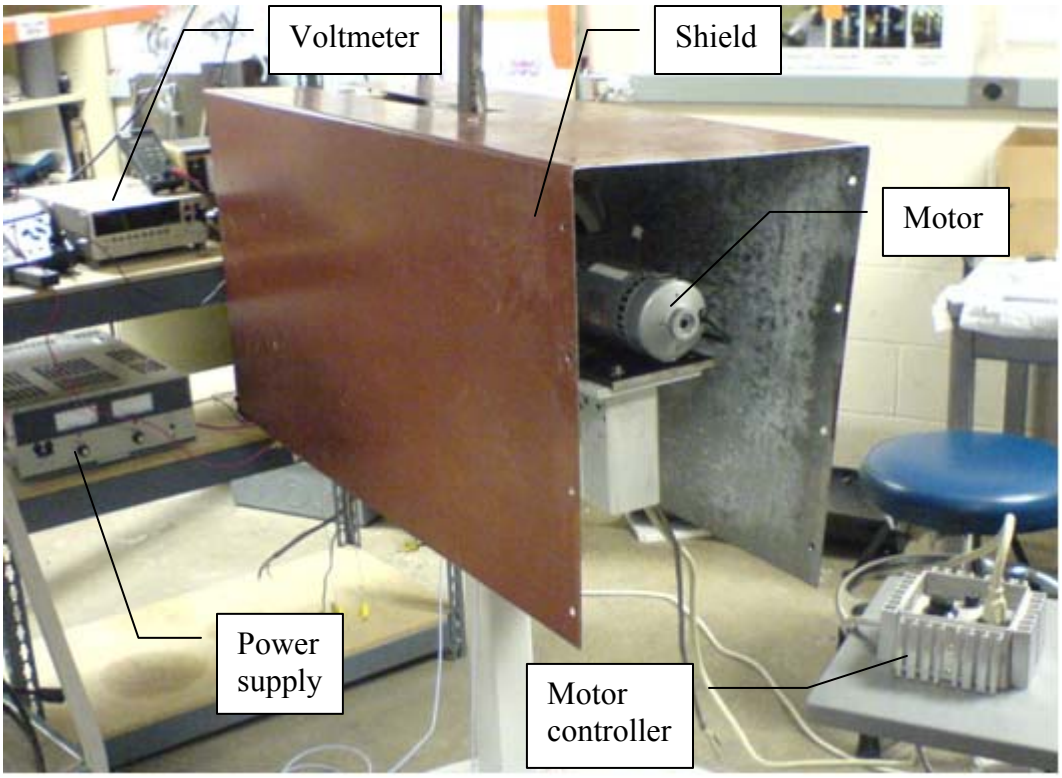

Figure 4.4 Experimental setup for testing at high speeds

A program was developed which could plot different graphs when the magnetic bearing is operated. A wire is connects the Bentley sensor controller and the computer in which the program is generated. When the magnetic bearing is operated the wire obtains the information from the sensor controller and is sent to the program which generates plots for various relations. The operating conditions are, 75 ^{0}F , 10A current, with a gap of 20 mils between the rotor and stator with silver coil, preload of 50 lbs. Speed was varied from 0 to 5500 rpm and then power was shut off. Figure 4.5 shows the relation between time and speed of the shaft. Just after 40 seconds there is sudden drop of speed as the power to the motor driving shaft is cut off.

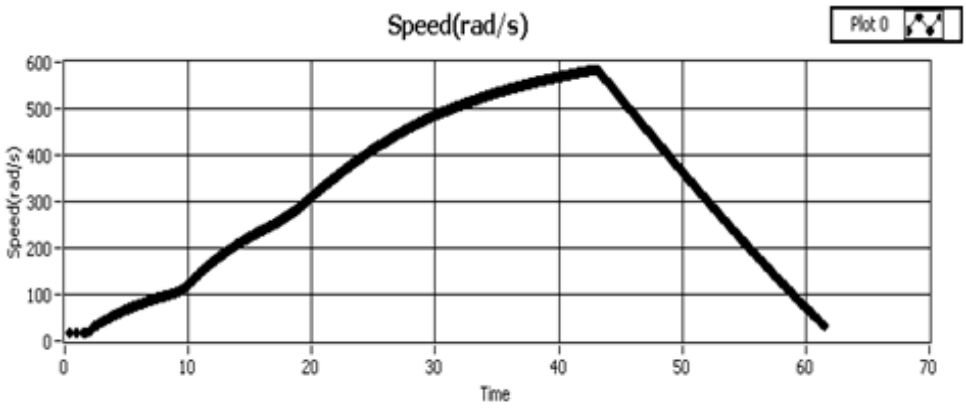

Figure 4.5 Speed vs time at room temperature, 10 A

Figure 4.6 shows the relation between acceleration of shaft and time, operated at room temperature, 10 A current by varying speed from 0 to 5500 rpm. Between 40 and 45 seconds there is sudden drop in acceleration as the power is shut off to the motor.

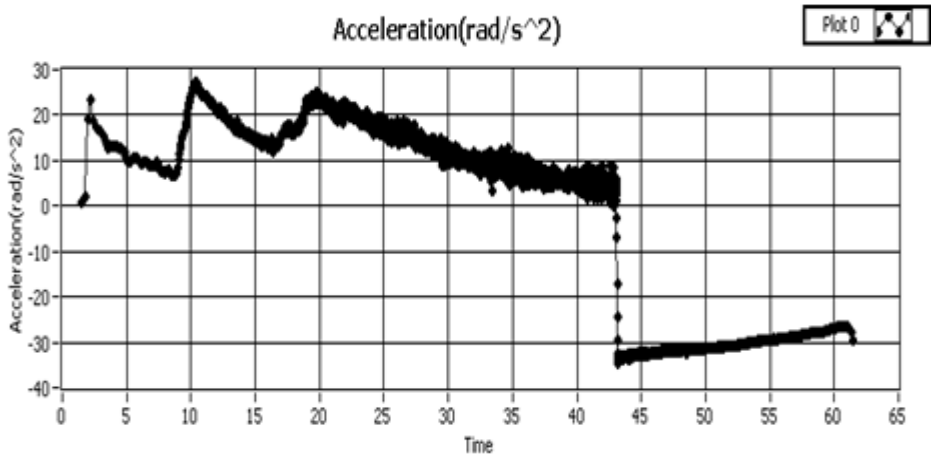

Figure 4.6 Acceleration of shaft by varying speed at room temperature, 10A

Figure 4.7 shows the power consumption of the shaft over time, when operating from 0 to 5500 rpm and then back to 0 rpm at room temperature and 10 A. The power required was calculated using the below formulae. Between 40 and 45 seconds there is sudden drop in acceleration as the power is shut off to the motor.

Power is defined as the angular velocity (ω) times the torque (T) required for operation, which is equal to the derivative of energy (E) over a period of time.

$$P = \omega * T \tag{4.1}$$

$$P = \frac{dE}{dt} \tag{4.2}$$

Energy in a rotating body is defined as the product of moment of inertia of the body (I_p) and the square of the angular velocity of the body.

$$E = \frac{1}{2} I_p \omega^2 \tag{4.3}$$

$$\frac{dE}{dt} = I_p \omega \dot{\omega} = Power \tag{4.4}$$

$I_p = 0.012892\ kg/m^2$ is calculated from the 3D model using SolidWorks.

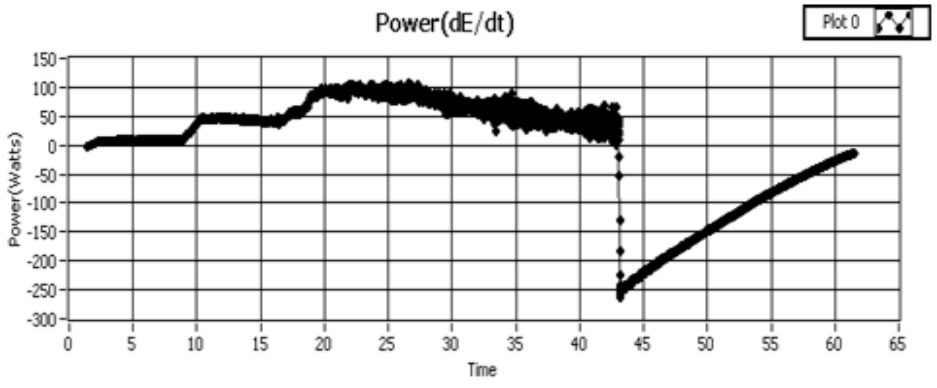

Figure 4.7 Power consumed by shaft vs time by varying speed at75^{0}F, 10A

Figure 4.8 shows the plot between power consumption and speed of the shaft when operating from 0 to 5500 rpm and then back to 0 rpm at room temperature and 10 A. Upper curve is when speed increases from 0 to 5500 rpm. Lower curve plots the shaft coming back to rest. Sudden drop of power shows the power cut off from the motor.

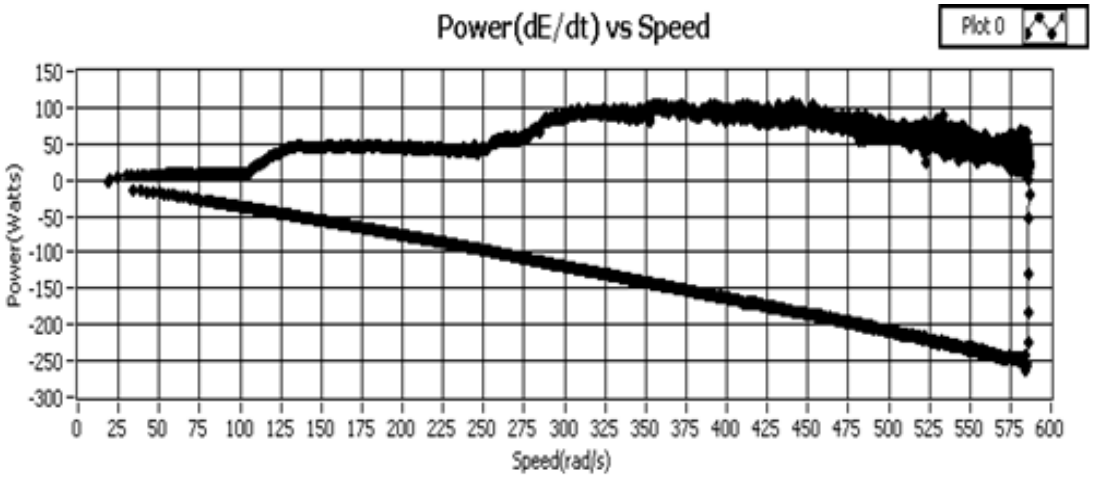

Figure 4.8 Power consumed by shaft vs speed at75^{0}F, 10A

Figure 4.9 shows the torque acting on the shaft over time, when operating from 0 to 5500 rpm and then back to 0 rpm at room temperature and 10 A. Between 40 and 45 seconds there is sudden drop in torque as the power is shut off to the motor.

Figure 4.10 shows the plot between torque and speed of the shaft when operating from 0 to 5500 rpm and then back to 0 rpm at room temperature and 10 A. Upper curve is when speed increases from 0 to 5500 rpm. Lower curve plots the shaft coming back to rest. Sudden drop of torque shows the power cut off from the motor.

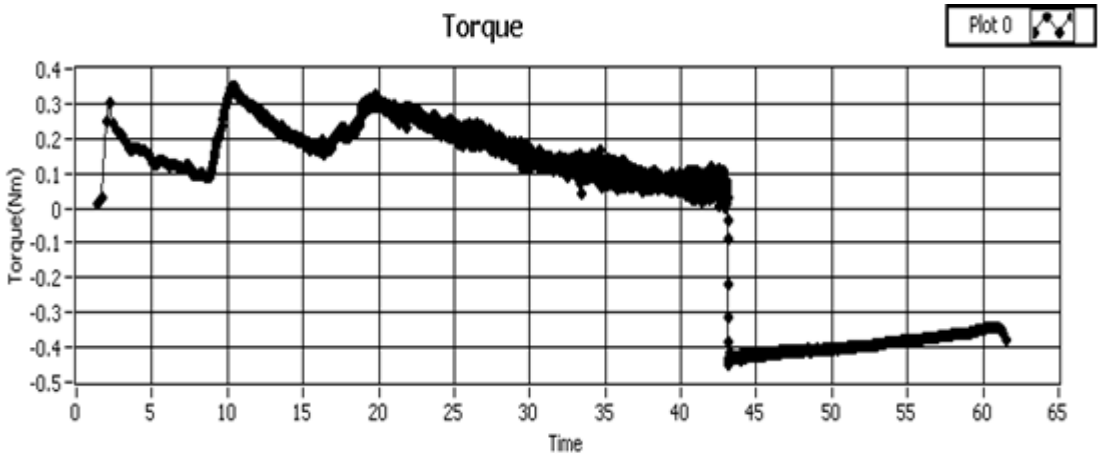

Figure 4.9 Torque on shaft vs time at varying speed from 0 to 5500 rpm at75^{0}F, 10A

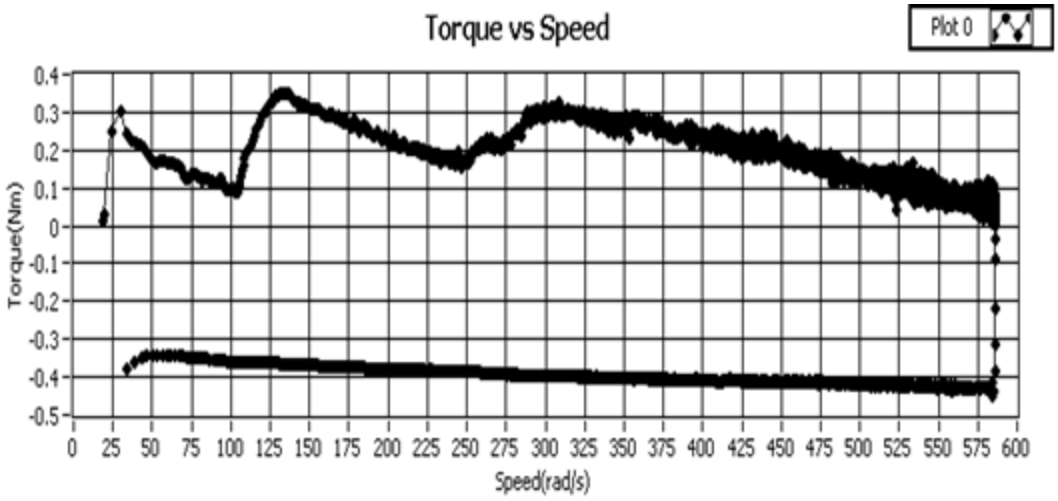

Figure 4.10 Torque on shaft vs speed at75^{0}F, 10A

Table 4.3 and Figure 4.11 show the values of forces by increasing speeds from 0 to 5000 rpm at 10A and room temperature. A preload of 50 lbs is applied on the load cell at 0 A. There is a gap of 20 mils between the rotor and the stator with silver coil. From the Figure 4.10 it is seen that force does not change due to the varying speed.

Table 4.3 Speed vs force at room temp (75 ^{0}F), 10 A, preload 50 lbs

Speed (RPM)	Force (Lbs)
0	1037.8
1000	1043.4
2000	1042
3000	1039.34
4000	1036.5
5000	1033.37
4000	1031.5
3000	1033.37
2000	1034.316
1000	1034.94
0	1040.9

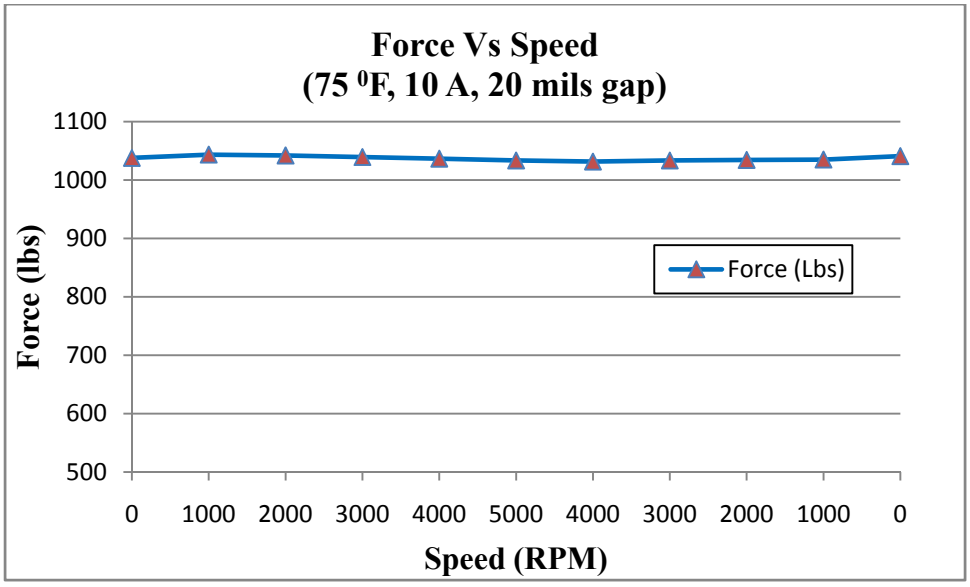

Figure 4.11 Speed vs force at room temp (75 ^{0}F), 10 A, preload 50 lbs

4.4 Tests and Results at High Temperatures and High Speeds

The most important testing phase is at combination of high speeds and high temperatures. Testing of magnetic bearing at high temperatures, high currents and high speeds is very risky. Proper care should be taken to prevent temperatures from exceeding the safe operating conditions. Load cell temperature is continuously monitored and kept below 140^0F by blowing cold air on it. Extra protection is placed around the shield. Figure 4.12 shows the extra protection around the cover.

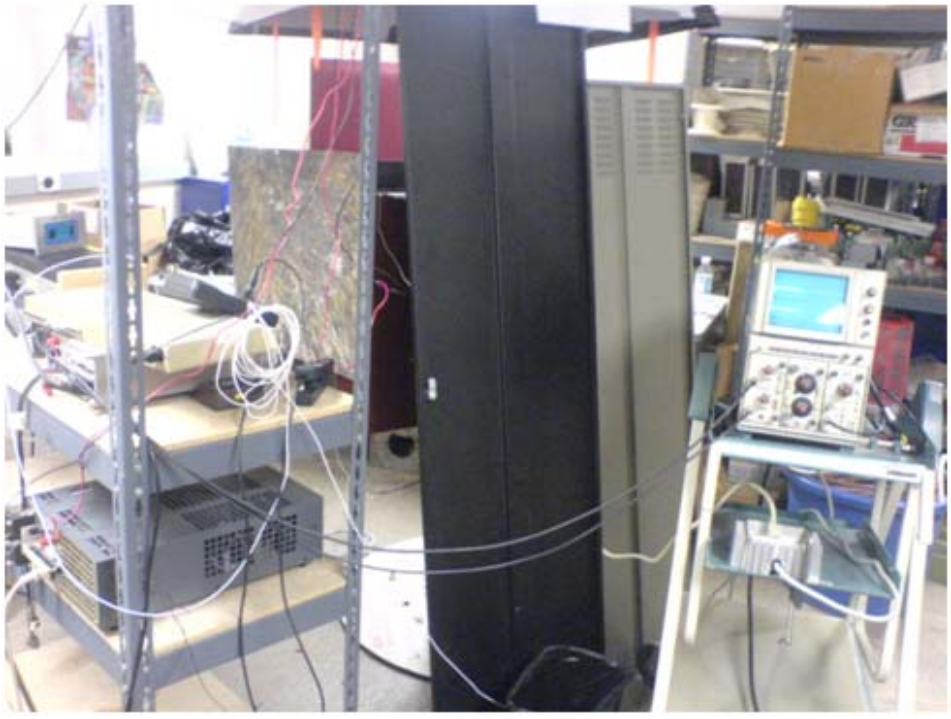

Figure 4.12 Set up for high temperatures and speeds

A duct is placed on the top of the magnetic bearing to remove the hot gases coming out during the high temperature operation. A motor is used to suck the gases and pump

them outside. A thick, non flammable cloth is also placed around to prevent gases from spreading in the lab. Figure 4.13 shows the inflammable cloth and the duct system.

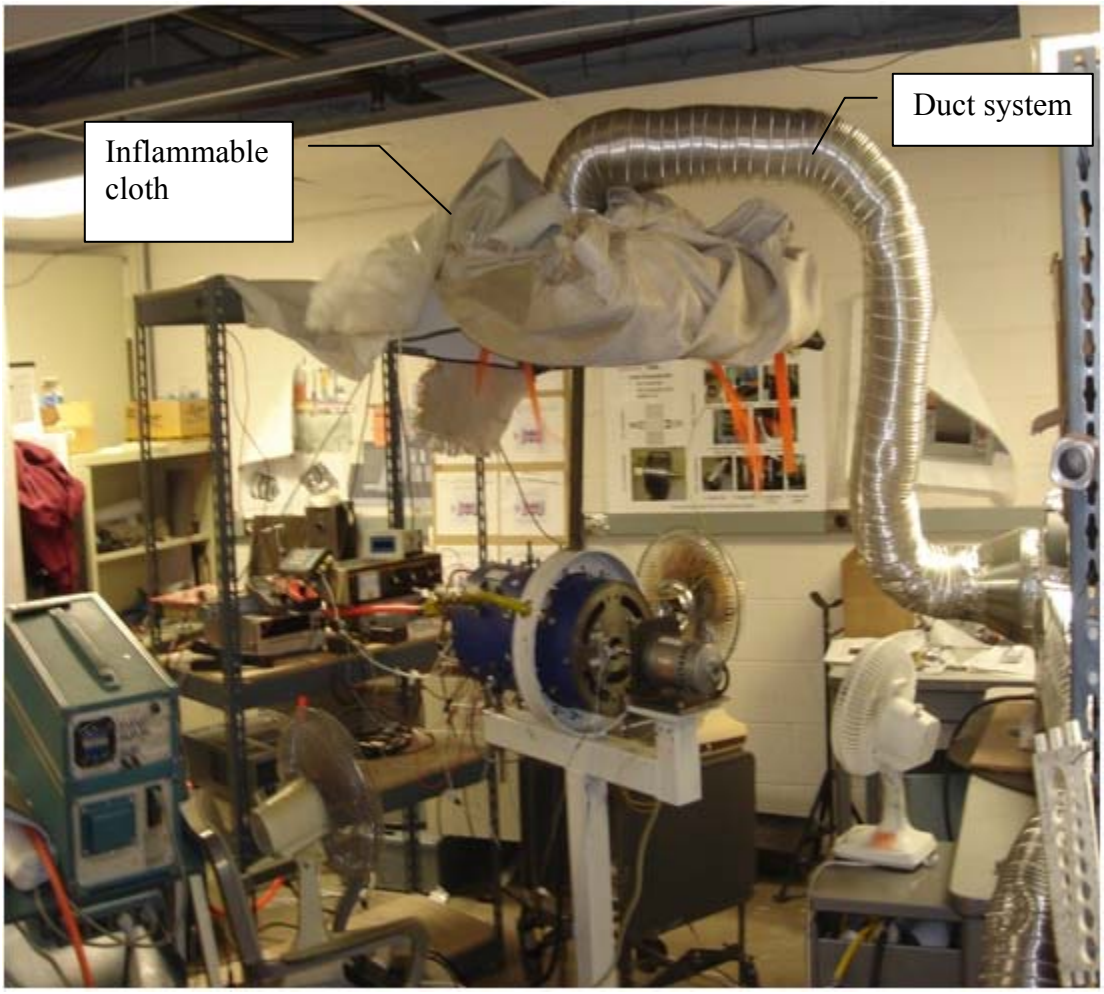

Figure 4.13 Set up for high temperature showing duct and inflammable cloth

Table 4.4 and Figure 4.14 show the force variation with current at 500 ^{0}F, speed of 0 and 1000 rpm. There is a preload at 0 A. There is a gap of 16 mils between the rotor and the stator with silver coil.

Table 4.4 Current vs force at 500 ^{0}F, varying current

	Tested Force (Lbs)	
Current (A)	**0 Rpm**	**1000 Rpm**
0	47.1	50
1	55.9	61.23
2	85.1	90.43
3	146.64	142.55
4	205.04	227
5	304.6	327.8
6	444	447.45
7	584.04	619.5
8	760.13	827.4
9	867	910.6
10	1007.94	1017.36
11	1116.27	1122.23
12	1185.35	1191

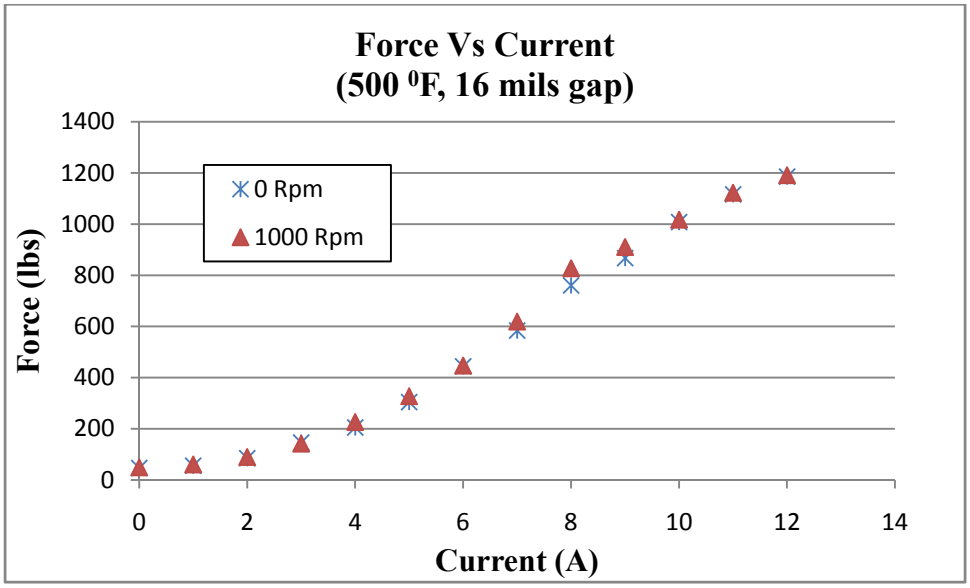

Figure 4.14 Current vs force at 500 ^{0}F, 0 RPM, varying current

Table 4.5 and Figure 4.15 show the force variation with speed at 500 ^{0}F, current of 10 A. There is a preload of 50 lbs at 0 A. There is a gap of 16 mils between the rotor and the stator with silver coil. From the graph it is seen that force is constant over varying speed.

Table 4.5 Speed vs force at 500 ^{0}F, 10 A, 16 mils gap

Speed (RPM)	Force (Lbs)
0	1016.6
1000	1020.31
2000	1023.23
3000	1012.27
4000	1007.91
5000	1014.57
4000	1018.48
3000	1016.84
2000	1014.34
1000	1015.71
0	1009.76

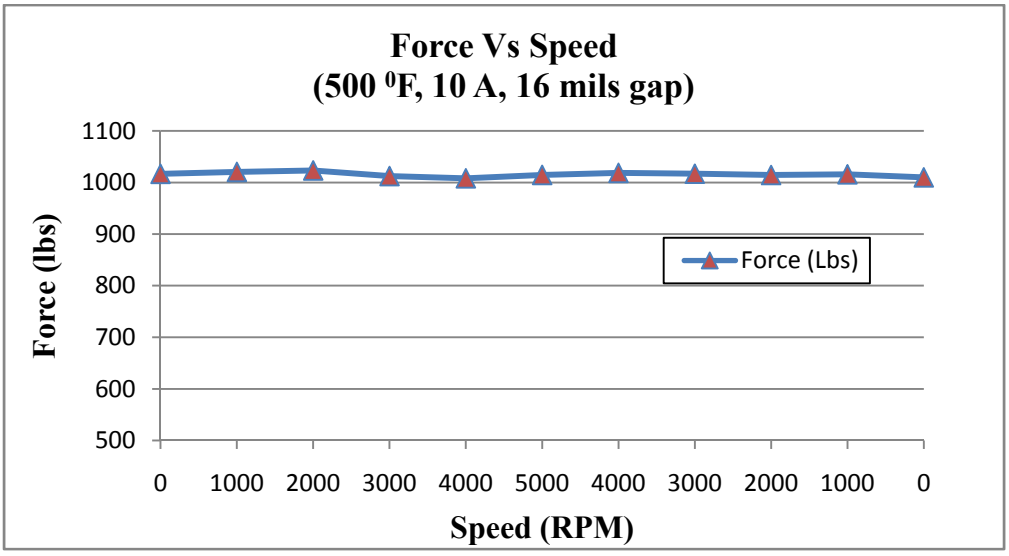

Figure 4.15 Force vs speed at 500 ^{0}F, 10 A, 16 mils gap

Table 4.6 and Figure 4.16 show the force variation with current at 1000 ^{0}F, room speeds of 0 and 2000 rpm. There is a preload at 0 A. There is a gap of 16 mils between the rotor and the stator with silver coil. Current is varied from 0 to 11 amps. Resistance in the coils increases as the temperature increases; due to which high voltage is required to obtain large currents. Current was restricted to 11 A due to unavailability of high voltage supply.

Table 4.6 Current vs force at 1000 ^{0}F, 16 mils gap

	Tested Force (Lbs)	
Current(A)	**0 Rpm**	**2000 Rpm**
0	45.8	48.7
1	50.9	55.9
2	72.2	70.33
3	103.76	103.6
4	163.3	159.5
5	263.76	260.6
6	386.22	343.5
7	568.34	533.8
8	719.06	706.5
9	803.8	785
10	885.5	882.34
11	976.54	967.12

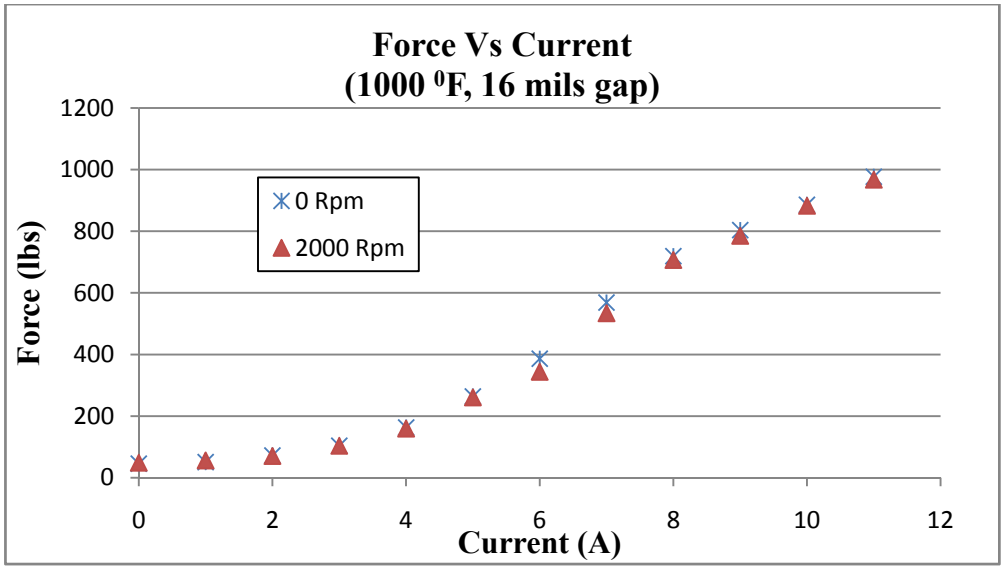

Figure 4.16 Current vs force at 1000 ^{0}F, 16 mils gap, varying current

Table 4.7 and Figure 4.17 show the force variation with speed at 1000 ^{0}F, constant current of 10 A. Gap of 16 mils is maintained between the rotor and stator with silver coil. Speed of shaft is varied from 0 to 5000 rpm and reduced to 0 rpm using a motor and motor controller. Graph shows that there is not much change in the force acting on the load cell by varying the speed.

Table 4.7 Speed vs force at 1000 ^{0}F, 10 A, 16 mils gap

Speed (RPM)	Force (Lbs)
0	864.44
1000	863.5
2000	863.5
3000	860.36
4000	860.36
5000	852.51

Table 4.7 Continued

Speed (RPM)	Force (Lbs)
4000	844.66
3000	847.8
2000	850.3
1000	850.94
0	856.6

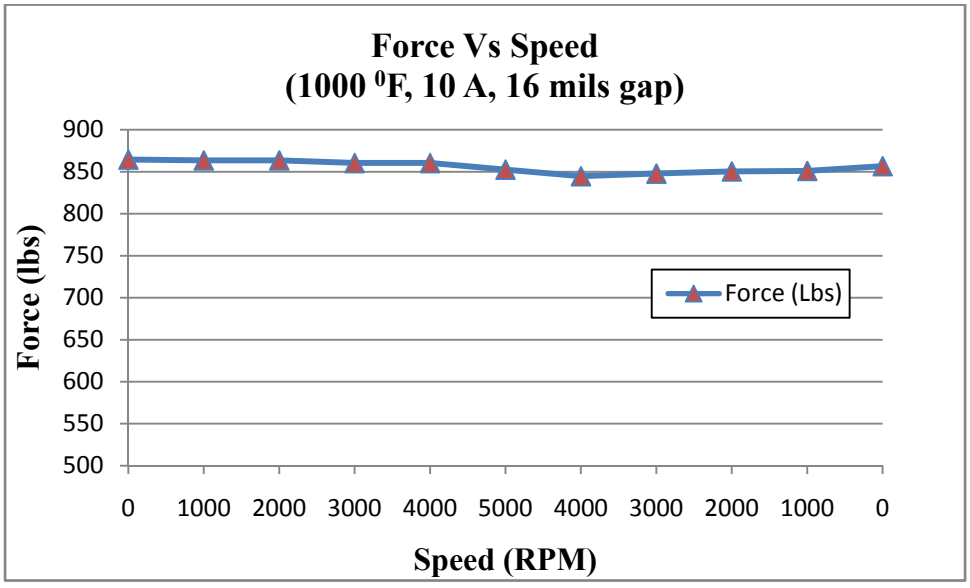

Figure 4.17 Speed vs force at 1000 ^{0}F and 10 amps

4.5 Uncertainty Analysis

Each measurement taken by an instrument includes some uncertainty. These individual uncertainties will create an uncertainty in the calculated result. Process of finding the uncertainty in a result caused due to uncertainties in the independent variables is called the propagation of uncertainty.

By approximating that *y* is a linear function of the independent variables ($x_1, x_2 \ldots x_n$) and each measured variable has some uncertainty ($u_1, u_2 \ldots u_n$) respectively, then the uncertainties will behave like standard deviations

$$u_y = \sqrt{\left(\frac{\partial y}{\partial x_1} u_1\right)^2 + \left(\frac{\partial y}{\partial x_2} u_2\right)^2 + \cdots + \left(\frac{\partial y}{\partial x_n} u_n\right)^2}$$

The uncertainties u_i can be either precision or bias uncertainties. For calculating the uncertainty of force in the magnetic bearing

$$F = \xi V$$

Where F = measured force

ξ = sensitivity of load cell

v = voltage

Uncertainty of load cell=1%

Uncertainty of voltmeter=3%

$$\Delta F = \Delta\xi * V + \Delta V * \xi$$

$$\frac{\Delta F}{F} = \frac{\Delta\xi}{\xi} + \frac{\Delta F}{F}$$

$$\left|\frac{\Delta F}{F}\right| = \sqrt{\left(\frac{\Delta\xi}{\xi}\right)^2 + \left(\frac{\Delta F}{F}\right)^2}$$

$$\left|\frac{\Delta F}{F}\right| = \sqrt{(1)^2 + (3)^2} = 3.16\%$$

This uncertainty in the measurement is mainly due to movement of loadcell from its position on force nut during the operation of the magnetic bearing.

4.6 Temperature Vs Resistance in Coils

Table 4.8 and Figure 4.18 show the increase in resistance in the coils due to increase in temperature. During high temperature operations we need to have a high voltage input in order to compensate the resistance and achieve high currents.

Table 4.8 Temperature vs resistance in coils

Temperature (Deg F)	**Resistance in coils (Ohms)**
250	2.75
300	2.96
350	3.18
400	3.41
450	3.63
500	3.83
550	4.07
600	4.3
650	4.53
700	4.77
750	5.01
800	5.25
850	5.48
900	5.72
950	6.06
1000	6.35

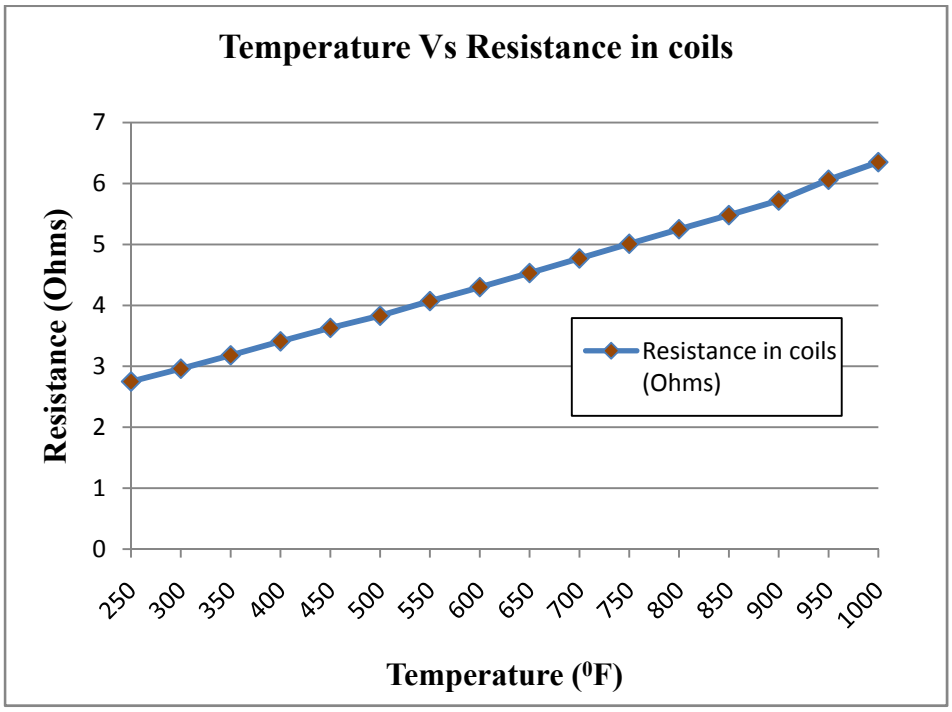

Figure 4.18 Temperature vs resistance in coils

CHAPTER V

PREDICTED RESULTS AND CORRELATION

5.1 1-D Magnetic Circuit Theory

The flux is circulated in a magnetic loop using an electromagnet or permanent magnet in the magnetic bearing technology. Per Ampere's law, the excitation is the product of current "i" and the number of complete loops "N" made. H is the magnetizing field.

$$\oint H.dl = Ni \tag{5.1}$$

$$\sum H_j L_j = \sum Ni \tag{5.2}$$

But, $H = \frac{B}{\mu}$

Where, B= magnetic field and μ= permeability of material

Substituting the equation (5.2) in equation (5.1), we get

$$\sum \frac{B_j}{\mu_j} L_j = \sum Ni \tag{5.3}$$

But, $B_j = \frac{\emptyset_j}{A_j}$;$\emptyset_1 = \emptyset_2 = \emptyset_3 = \cdots = \emptyset$

Where, Ø= flux

Therefore, $\emptyset \sum \frac{L_j}{\mu_j A_j} = \sum Ni$

$$\sum R_j \emptyset = \sum Ni$$

Reluctance $R_j = \frac{L_j}{\mu_j A_j}$

$$\therefore \phi_0 = \frac{N_0}{\sum\left(\frac{L_j}{\mu_j A_j}\right)}$$

To simplify the calculations all metal path reluctance is dropped.

If $N_0 = N_I = N$ and $i_I = i_0$

Therefore $\emptyset = \emptyset_0 = \emptyset_I = \frac{Ni}{\left(\frac{2g}{\mu_0 A}\right)}$

Where, g=gap

Therefore, $B = \frac{\emptyset}{A} = \frac{Ni\mu_0}{2g}$ (5.4)

For accounting the fringing and leakage losses a derate fator "β" is introduced in equation (5.4)

Therefore, $B = \frac{Ni\mu_0}{2g} * \beta$ (5.5)

From Maxwell stress sensor, $\tilde{F} = \frac{B^2 A}{2\mu_0}$

Figure 5.1 taken from [1] shows the magnetic force distribution in a stator.

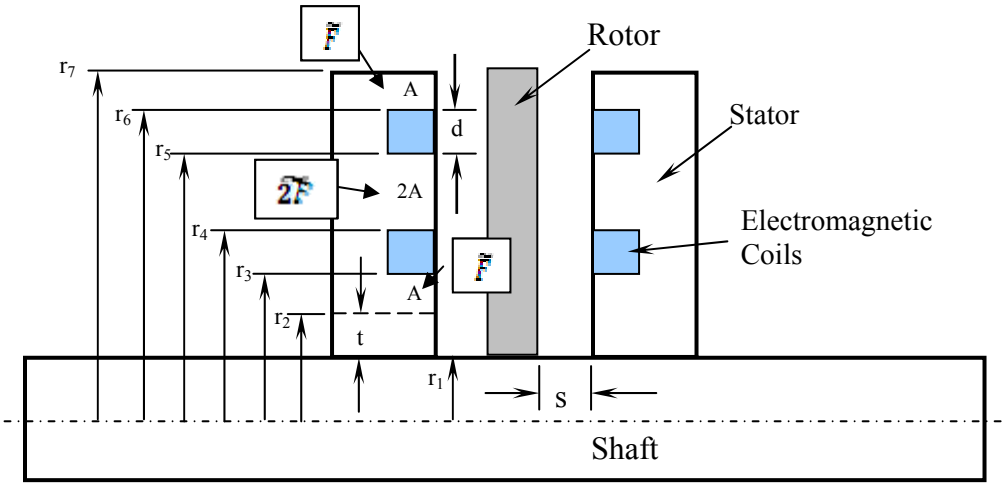

Figure 5.1 Magnetic force distribution in a stator

Total magnetic force, $F = 4\tilde{F} = 4 * \frac{B^2 A}{2\mu_0}$ (5.6)

Substituting equation (5.5) in equation (5.6)

$$F = \frac{4A}{2\mu_0} \frac{N^2 i^2 \mu_0^2}{4g^2} \beta^2 = \frac{A\mu_0 N^2 i^2}{2g^2} \beta^2$$

Therefore, $F = \frac{A\mu_0 N^2 i^2}{2g^2} \beta^2$ (5.7)

Mohiuddin [6] determined, A = area of the air gap = 27.95 cm^2

N = no. of turns of wire = 100

i = current supplied = 1, 2… 15 amps

g = gap between the rotor and stator with silver coil.

μ_0= permeability of free space = $4\pi * 10^{-7}$ NA^{-2}

Theoretical calculations are made using the equation (5.7). By varying the gap and current, force is calculated. Derate factor of 0.8 is employed often to account for the 1D nature of the magnetic circuit model to account for fringing and leakage.

Table 5.1 and Figure 5.2 show the predicted forces for various gaps between stator and rotor with varying current.

Table 5.1 Predicted forces for various gaps between stator and rotor

	Predicted Force (Lbs)			
Current (A)	**Gap 16 mils**	**Gap 18 mils**	**Gap 20 mils**	**Gap 25 mils**
0	0.0	0.0	0.0	0.0
1	23.9	18.9	15.3	9.8
2	95.6	75.5	61.2	39.2
3	215.1	170.0	137.7	88.1
4	382.5	302.2	244.8	156.7
5	597.6	472.2	382.5	244.8
6	860.5	679.9	550.7	352.5
7	1171.3	925.5	749.6	479.8
8	1529.9	1208.8	979.1	626.6
9	1936.2	1529.8	1239.2	793.1
10	2390.4	1888.7	1529.9	979.1
11	2892.4	2285.3	1851.1	1184.7
12	3442.2	2719.7	2203.0	1409.9
13	4039.8	3191.9	2585.4	1654.7
14	4685.2	3701.9	2998.5	1919.0
15	5378.4	4249.6	3442.2	2203.0

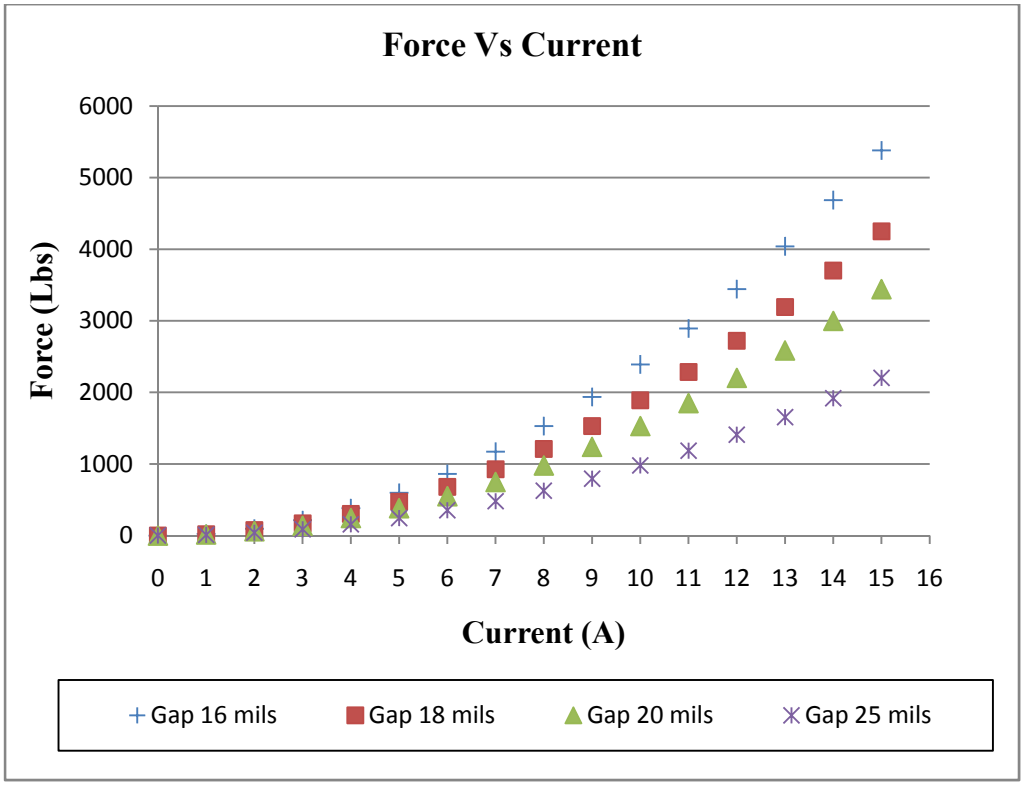

Figure 5.2 Predicted forces for various gaps between stator and rotor

5.2 Correlation between Predicted Results and Test Results at Room Temperature

Test results shown in chapter IV which are obtained during the operation of magnetic thrust bearing at various conditions are compared with the results obtained from the 1D magnetic circuit theory. Table 5.2 and Figure 5.3 show the calculated forces with a derate factor (β) and test forces for operating conditions room temperature (75 ^{0}F), gap of 25 mils between the rotor and stator with silver coil, 0 rpm with varying current. Graph shows that at room temperature, test results vary between the predicted results with β=0.8 and β=0.85.

Table 5.2 Calculated forces and tested forces at 75 ^{0}F, 25 mils gap, 0 rpm

		Predicted forces (Lbs)			
Current (A)	**Tested Force (Lbs)**	**Predicted force (lbs), β=0.75**	**Predicted force (lbs), β=0.8**	**Predicted force (lbs), β=0.85**	**Predicted force (lbs), β=1**
0	0	0	0	0	0
1	1.9	5.51	6.27	7.07	9.79
2	10.7	22.03	25.06	28.3	39.16
3	38	49.57	56.4	63.67	88.12
4	88.23	88.12	100.26	113.18	156.66
5	154.5	137.69	156.66	176.85	244.78
6	229.9	198.27	225.58	254.66	352.48
7	318.1	269.86	307.05	346.63	479.76
8	435.52	352.48	401.04	452.74	626.62
9	570.9	446.1	507.57	572.99	793.07
10	723.8	550.74	626.62	707.4	979.1
11	848.43	666.4	758.22	855.95	1184.71
12	947	793.07	902.34	1018.66	1409.9
13	1033.1	930.76	1058.99	1195.51	1654.68

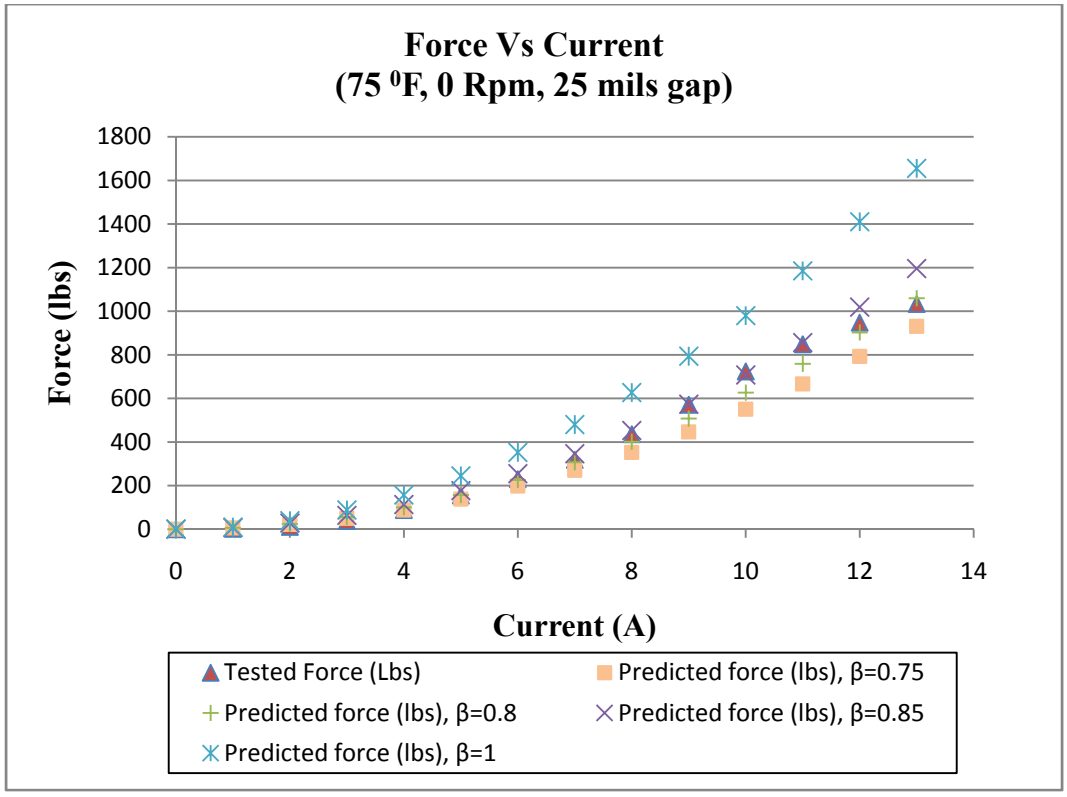

Figure 5.3 Calculated and predicted forces with varying currents at 75 F, 0 rpm, 25 mils

Table 5.3 and Figure 5.4 show the calculated forces with a derate factor (β) and test forces. The operating conditions are room temperature (75 ^{0}F), gap of 20 mils between the rotor and stator with silver coil, 0 rpm with varying current. Graphs show that at room temperature test results vary between the predicted results with β=0.7 and β=0.8.

Table 5.3 Calculated forces and tested forces at 75 ^{0}F, 20 mils gap, 0 rpm

		Predicted force (Lbs)			
Current (A)	**Tested Force (Lbs)**	**β=0.7**	**β=0.75**	**β=0.8**	**β=1**
0	0	0	0	0	0
1	1.9	7.5	8.61	9.79	15.3
2	13.5	29.99	34.42	39.16	61.19
3	57.8	67.47	77.45	88.12	137.69
4	124.7	119.94	137.69	156.66	244.78
5	207.24	187.41	215.14	244.78	382.46
6	301.44	269.87	309.79	352.48	550.75
7	414.5	367.32	421.66	479.76	749.63
8	565.9	479.76	550.75	626.63	979.1
9	731.6	607.2	697.04	793.07	1239.18
10	868.2	749.63	860.54	979.1	1529.85
11	970.9	907.05	1041.25	1184.72	1851.12
12	1062.6	1079.46	1239.18	1409.91	2202.98

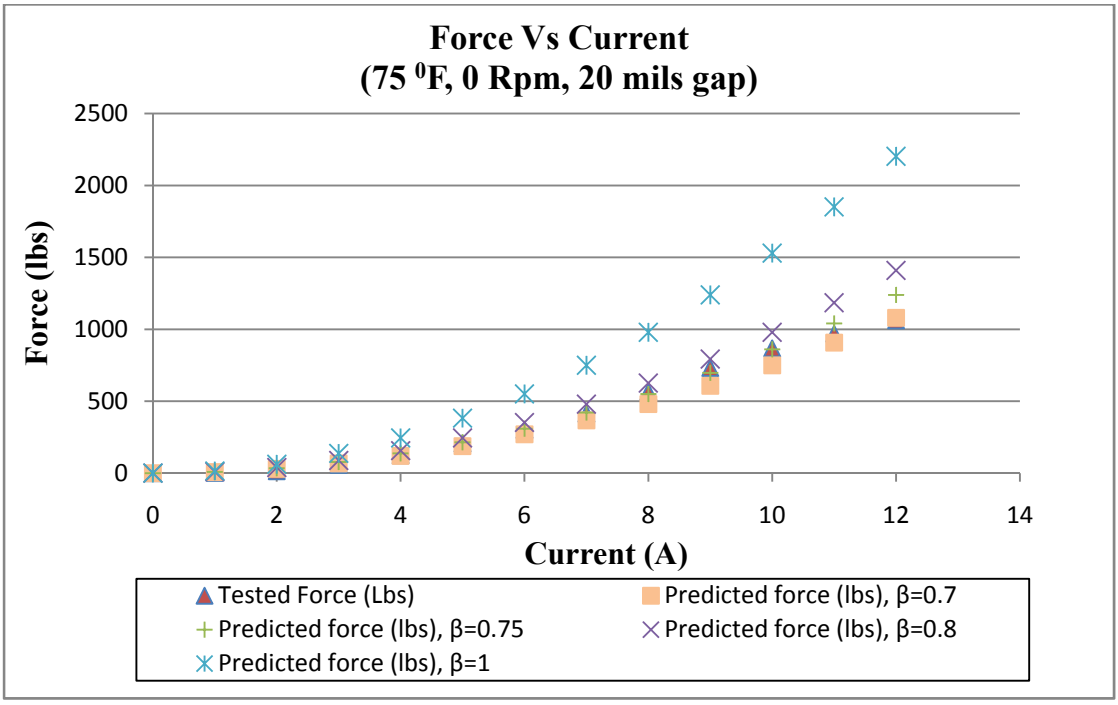

Figure 5.4 Calculated and predicted forces with varying currents at 75 F, 0 rpm, 20 mils

Table 5.4 shows the calculated forces and test forces with varying speeds. Operating conditions are 75 ^{0}F, gap of 20 mils between the rotor and stator with silver coil, with constant current of 10 A. The Figure 5.5 shows the calculated forces, test forces and Dr Kenny's prediction [11] with varying speeds. Graphs show that test results and calculated results are uniform with varying speeds. This shows that speed has no effect on the thrust forces.

Table 5.4 Calculated forces and tested forces at 75 ^{0}F, 20 mils gap, 10 A

Speed (RPM)	**Tested Force (Lbs)**	**Predicted force (lbs), β=0.8**	**Predicted force (lbs), β=1**
0	987.8	979.1	1529.85
1000	993.4	979.1	1529.85
2000	992	979.1	1529.85
3000	989.34	979.1	1529.85
4000	986.5	979.1	1529.85
5000	983.37	979.1	1529.85
4000	981.5	979.1	1529.85
3000	983.37	979.1	1529.85
2000	984.316	979.1	1529.85
1000	984.94	979.1	1529.85
0	990.9	979.1	1529.85

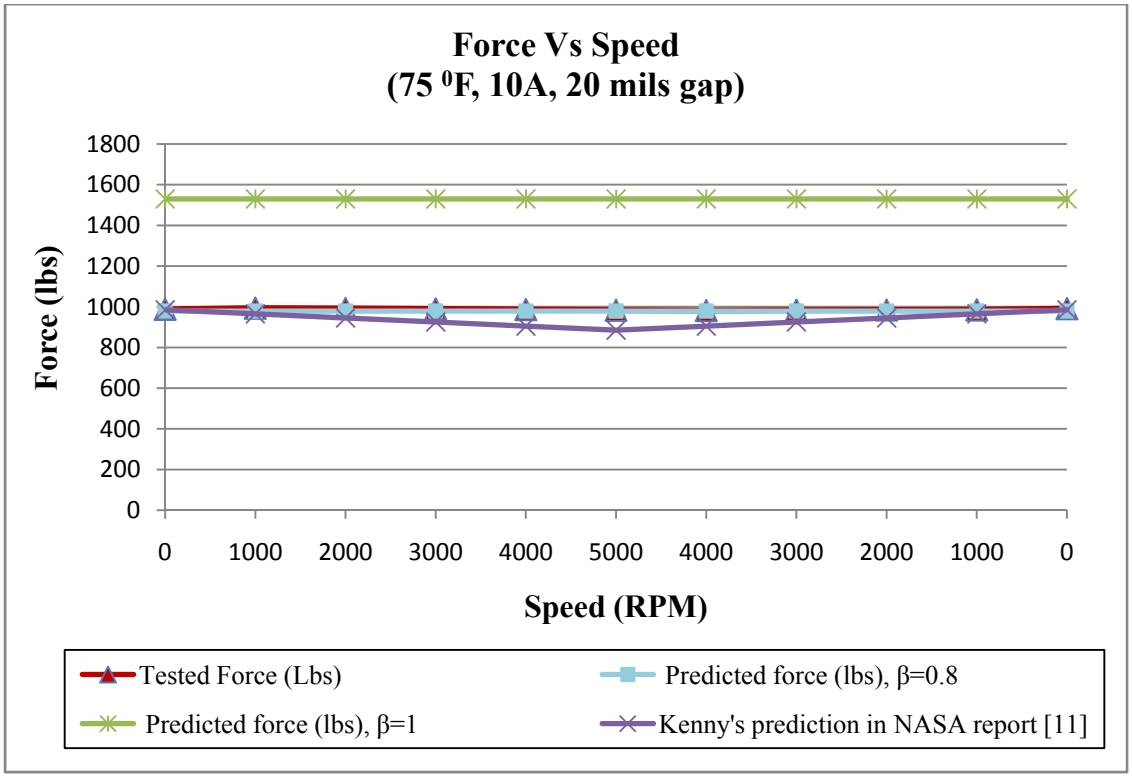

Figure 5.5 Calculated and predicted forces with varying speed, at 10 A, 75 ^{0}F, 20 mils

5.3 Correlation between Predicted Results and Test Results at High Temperatures

Predicting the results at high temperatures is always very hard. There are many things that can affect the actual test results to be different to the predicted results. Derate factor value decreases when the temperatures increases to accommodate the decrease of permeability of the stator and rotor materials. In addition there is increase of leakages and fringing losses due to the stresses induced, thermal expansion of metals, human errors due to difficulty of operation at such high temperatures etc. Table 5.5 and Figure 5.6 show the calculated forces (with derate factors) and test forces. Operating conditions

are 500 ^{0}F, gap of 16 mils between the rotor and stator with silver coil, with varying current at speeds of 0 and 1000 rpm. From the graphs in Figure 5.6 it was observed that tested forces at 0 and 1000 rpm are between the predicted forces with β=0.65 and β=0.7. At higher currents there is a fall of tested forces, this was attributed to the tilting of the rotor due to inability of the support bolts to withstand such extreme operating conditions.

Table 5.5 Calculated forces and tested forces at 500 ^{0}F, 16 mils gap and 0, 1000 rpm

	Tested Force (Lbs)		**Predicted Force (Lbs)**		
Current (A)	**0 Rpm**	**1000 Rpm**	**β=0.65**	**β=0.7**	**β=1**
0	0	0	0	0	0
1	8.8	11.23	10.1	11.71	23.9
2	38	40.43	40.4	46.85	95.62
3	99.54	92.55	90.89	105.42	215.14
4	157.94	177	161.59	187.41	382.46
5	257.5	277.8	252.49	292.82	597.6
6	396.9	397.45	363.58	421.67	860.54
7	536.94	569.5	494.87	573.94	1171.3
8	713.03	777.4	646.36	749.63	1529.86
9	819.9	860.6	818.05	948.75	1936.22
10	960.84	967.36	1009.94	1171.3	2390.4
11	1069.17	1072.23	1222.03	1417.27	2892.38

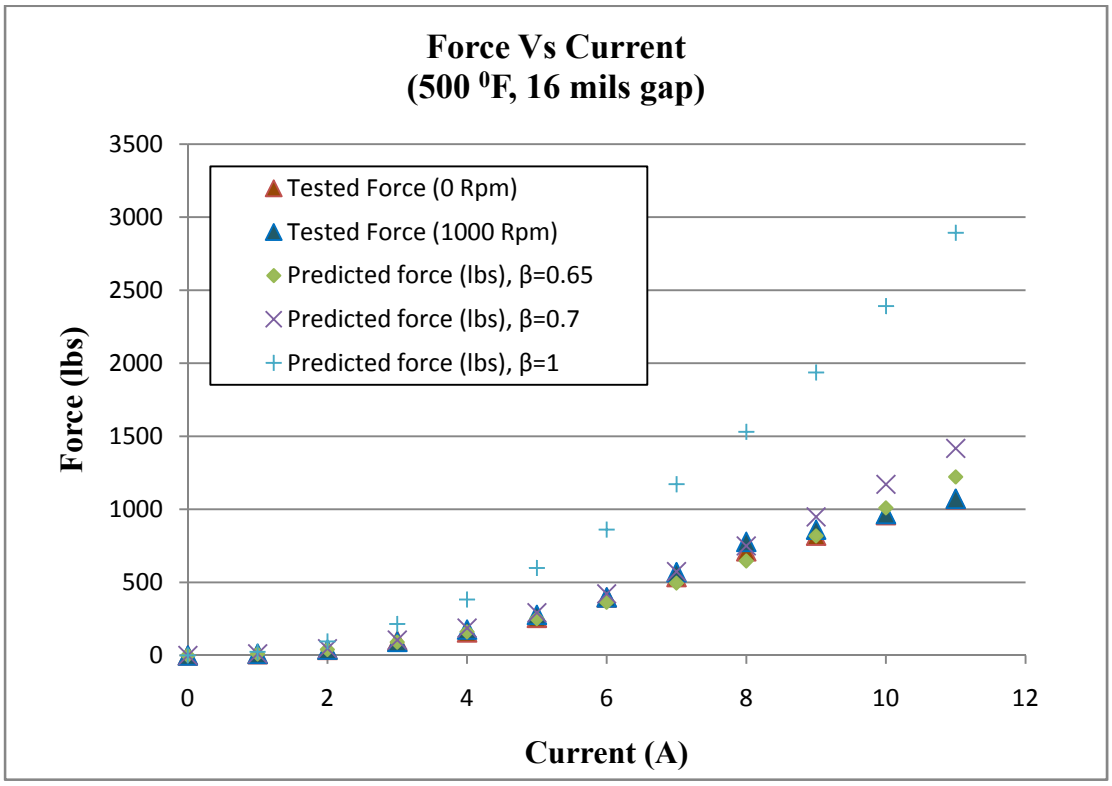

Figure 5.6 Calculated and predicted forces at 500 ^{0}F, 16 mils gap and 0, 1000 rpm

Table 5.6 and Figure 5.7 show the calculated forces and test forces with constant current of 10A. Operating conditions are 500 ^{0}F, 16 mils between the rotor and stator with silver coil, with varying speed. Graphs in Figure 5.7 show that, test results and calculated results are uniform with varying speeds. This shows that speed has no effect on the thrust forces.

Table 5.6 Calculated forces and tested forces at 500 ^{0}F, 16 mils gap, 10 A

Speed (RPM)	Tested force (lbs)	Predicted force (lbs), β=0.65	Predicted force (lbs), β=1
0	969.6	1009.94	2390.4
1000	973.31	1009.94	2390.4
2000	976.23	1009.94	2390.4
3000	965.27	1009.94	2390.4
4000	960.91	1009.94	2390.4
5000	967.57	1009.94	2390.4
4000	971.48	1009.94	2390.4
3000	969.84	1009.94	2390.4
2000	967.34	1009.94	2390.4
1000	968.71	1009.94	2390.4
0	962.76	1009.94	2390.4

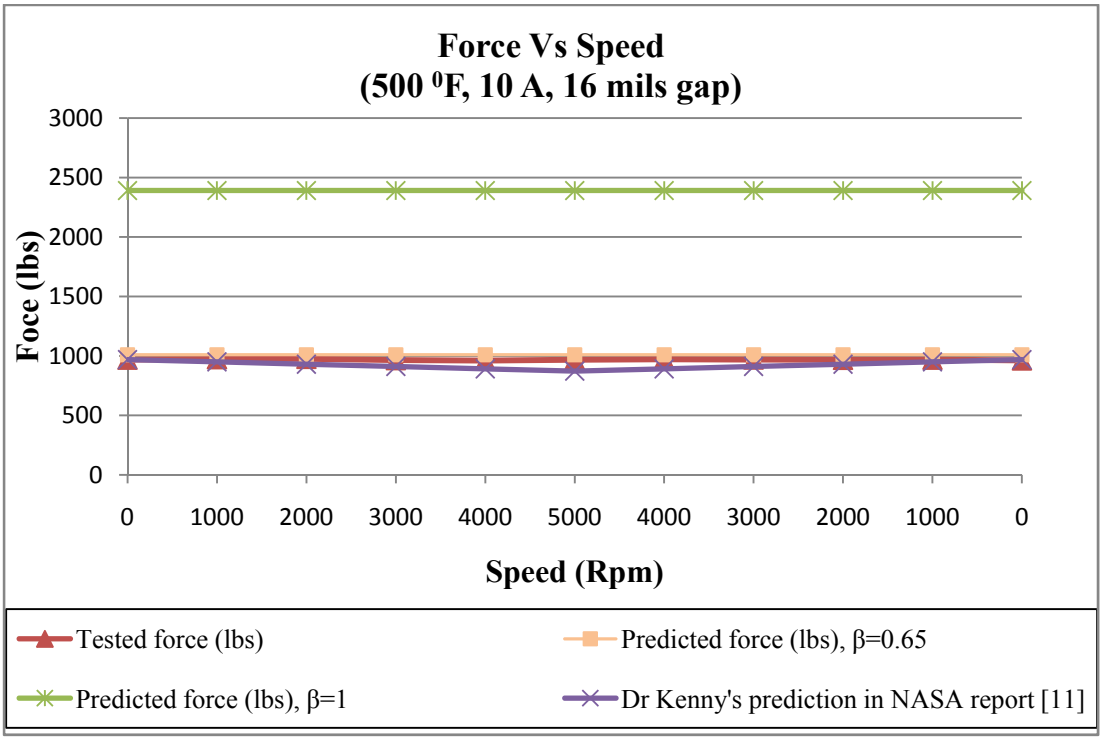

Figure 5.7 Calculated forces and tested forces at 500 ^{0}F, 16 mils gap, 10 A

Table 5.7 and Figure 5.8 show the calculated forces (with derate factors) and test forces at 0 rpm and 2000 rpm. Operating conditions are 1000 ^{0}F, gap of 16 mils between the rotor and stator with silver coil, and varying current. From the graphs it is observed that tested forces at 0 and 2000 rpm are equal to the predicted forces with β=0.6 and β=0.65. At higher currents there is a fall of tested forces, this can be attributed to the tilting of the rotor due to inability of the support bolts to withstand such extreme operating conditions.

Table 5.7 Calculated forces and tested forces at 1000 ^{0}F, 16 mils gap and 0, 2000 rpm

	Tested Force (Lbs)		**Predicted Force (Lbs)**		
Current(A)	**0 Rpm**	**2000 Rpm**	**β=0.60**	**β=0.65**	**β=1**
0	0	0	0	0	0
1	5.1	7.2	8.61	10.1	23.9
2	26.4	21.63	34.42	40.4	95.62
3	57.96	54.9	77.45	90.89	215.14
4	117.5	110.8	137.69	161.59	382.46
5	217.96	211.9	215.14	252.49	597.6
6	340.42	294.8	309.8	363.58	860.54
7	522.54	485.1	421.67	494.87	1171.3
8	673.26	657.8	550.75	646.36	1529.86
9	758	736.3	697.04	818.05	1936.22
10	839.7	833.64	860.54	1009.94	2390.4
11	930.74	918.42	1041.26	1222.03	2892.38

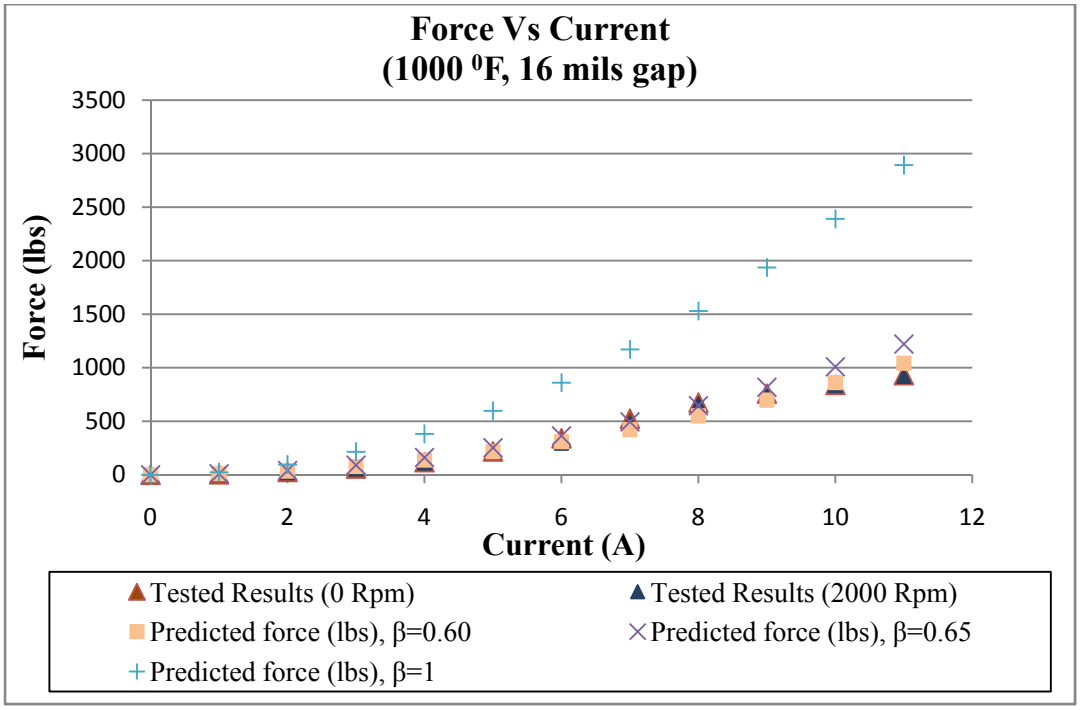

Figure 5.8 Calculated forces and tested forces at 1000 ^{0}F, 16 mils gap and 0, 2000 rpm

Table 5.8 and Figure 5.9 show the calculated forces and test forces with constant current of 10 A. Operating conditions are 1000 ^{0}F, 16 mils between the rotor and stator with silver coil, with varying speed. Graphs in Figure 5.9 show that, test results and calculated results are uniform with varying speeds. This shows that speed has no effect on the thrust forces.

Table 5.8 Calculated forces and tested forces at 1000F, 16 mils gap, 10 A

Speed (RPM)	Tested force (lbs)	Predicted force (lbs), β=0.6	Predicted force (lbs), β=1
0	864.44	860.54	2390.4
1000	863.5	860.54	2390.4
2000	863.5	860.54	2390.4

Table 5.8 Continued

Speed (RPM)	Tested force (lbs)	Predicted force (lbs), β=0.6	Predicted force (lbs), β=1
3000	860.36	860.54	2390.4
4000	860.36	860.54	2390.4
5000	852.51	860.54	2390.4
4000	844.66	860.54	2390.4
3000	847.8	860.54	2390.4
2000	850.3	860.54	2390.4
1000	850.94	860.54	2390.4
0	856.6	860.54	2390.4

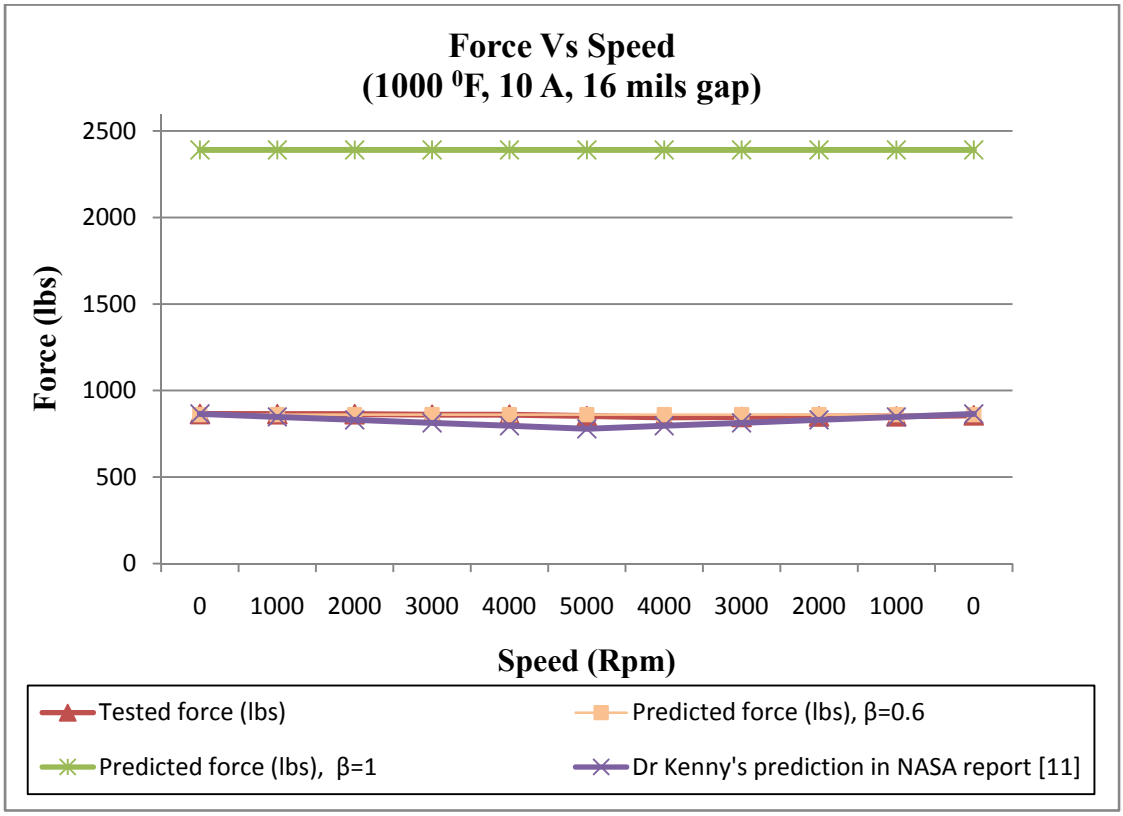

Figure 5.9 Calculated forces and tested forces at 1000 ^{0}F, 16 mils gap, 10 A

CHAPTER VI

CONCLUSION AND RECOMMENDATION

This thesis sought to answer the question whether it was possible to assemble and test the thrust magnetic bearing at operating conditions set by NASA. Below are the conditions set by NASA:

(a) Operating temperature of 538 ^{0}C (1000 ^{0}F).

(b) Rotational speeds of 25000 rpm.

(c) 4448 N (1000 lb-f) of axial thrust.

The high temperature axial thrust bearing was assembled and tested successfully.

Following are the correlation results from comparing the predicted/calculated results to the tested results:

1. At room temperature, spinning at 0 rpm and gap of 20 and 25 mils, tested results of the magnetic bearing are almost equal to the predicted forces with a derate factor (β) varying between 0.75 and 0.85.
2. As temperatures are increased magnetic forces are reduced. This is observed when we see that the test forces of room temperature and 20 mils are equal to the test forces at high temperatures and 16 mils.
3. At high temperatures (500 and 1000 ^{0}F) and constant operating speeds it is observed that magnetic forces are reduced. Test results are equal to the predicted results with a derate factor (β) varying between 0.6 and 0.65.

4. At all temperatures (room temp., high temp.), with a constant current of 10 A, both test and predicted results show no change in force when the speed is varied. Dr Kenny [11], had predicted that there will be a drop of 50 % axial thrust force at 30000 rpm high due to the motion induced eddy currents.

The results of research showed that:

1. Thrust magnetic bearing is capable of withstanding 1000 ^{0}F and withstand 1000 lb-f.
2. Thrust magnetic force does not decrease when operated at high speeds.
3. Hyperbolic profile rotor is very hard to align during operation.

The maximum operating speeds reached in this research are 5500 rpm. Due to safety considerations magnetic bearing was not operated at higher speeds.

Future work in this area includes measuring the axial load capacity under higher speeds and load conditions. Research needs to be done to see if there exists another actuator profile (non-hyperbolic) satisfying all NASA requirements.

REFERENCES

[1] Schweitzer, G., Bleuler, H., and Traxler, A., 1994, "Basics, Properties and Applications of Active Magnetic Bearings," Active Magnetic Bearings, Vol.1, pp. 1-112.

[2] Allaire, P. E., Mikula, A., Banerjee, B. B., Lewis, D. W., and Imlach, J., 1989, "Design and Test of a Magnetic Thrust Bearing", Journal of the Franklin Institute, Vol.326, pp.831-847.

[3] Ohsawa, M., Yoshida, K., Furuya, T., Marui, E., and Ninomiya, H., 1998, "High Temperature Blower for Molten Carbonate Fuel Cell Supported by Magnetic Bearing," *Proc. 6th Internat. Symp. on Magnetic Bearings*, MIT Cambridge, August 5-7, pp. 32-41.

[4] Mekhiche, M., Nichols, S., Oleksy, J., Young, J., Kiley, J., and Havenhill, D., 2000, "50K rpm, 1100°F Magnetic Bearings for Jet Tturbine Engines," *Proc. 7th Internat. Symp. on Magnetic Bearings*, ETH Zurich, Switzerland, August 23-25, 123-128.

[5] Harner, L. L., Dietrich D. W., and Masteller M. S., "An Overview of Soft Magnetic Materials for Magnetic Bearings", available at www.cartech.com, accessed on December 18, 2007.

[6] Mohiuddin, M., "Design of high Temperature high Speed Electromagnetic Axial Thrust Bearing," M.S. Thesis, Texas A&M University, Department of Mechanical Engineering, 2002.

[7] Hossain, M., "High Temperature, Permanent Magnet Biased, Homopolar Magnetic Bearing Actuator" M.S. Thesis, Texas A&M University, Department of Mechanical Engineering, 2006.

[8] Provenza, A., Montague, G., Jansen, M., Palazzolo, A., and Jansen, R., 2005, "High Temperature Characterization of a Radial Magnetic Bearing for Turbomachinery," Journal of Engineering for Gas Turbines and Power, **127,** pp.437-444.

[9] Kenny, A., and Palazzolo, A., 2003, "Single Plane Radial, Magnetic Bearings Biased with Poles Containing Permanent Magnets", Transactions of the ASME, **125**, pp. 178-185.

[10] Young, W. C., 2002, "*Roark's Formulas for Stress and Strain"*, 7th Edition, McGraw Hill, Inc., New York.

[11] Palazzolo, A., Kenny, A., Sun, G., Mohiuddin, W., Thomas, E., Tucker, R., Preuss, J., Kaushik, N., Subramaniyam, L., and Sifford, C., "High Temperature Magnetic Bearing – Blade Loss Mitigation", NRA-GRC-99-02- 18 month Milestone Review, April 04, 2003, NASA Glenn Research Center, pp. 93-105.

Supplementary Sources Consulted

Allaire, P. A., Fittro, R., Maslen, E., and Wakefield, E., 1994, "Eddy Current, Magnetic Flux and Force in Sold Magnetic Thrust Bearings," 4th Internat. Symp. of Magnetic Bearings, Zurich, Switzerland, pp. 157-163

Allaire, P. A., Fittro, R. L., Maslen, E., and Wakefield, W. C., 1997, “Measured Force / Current Relations in Solid Magnetic Thrust Bearings,” Journal of Engineering for Gas Turbine and Power, Vol.119, pp. 137-142

Baun, D. O., Fittro, R. L., and Maslen, E. H., 1997, "Force versus Current and Air Gap Calibration of a Double Acting Magnetic Thrust Bearing," ASME Journal of Engineering for Gas Turbines and Power, Vol.119, No. 4, October, pp. 942-948.

DeWeese, R. T., 1996, “A Comparison Study of Eddy Current Effects in a Single Sided Magnetic Thrust Bearing,” M.S. Thesis, Texas A&M University, Department of Mechanical Engineering.

Kelleher, W. P., and Kondoleon, A. S., 1997, “A Magnetic Bearing Suspension System for High Temperature Gas Turbine Applications”, Proc. Industrial Conference and Exhibition on Magnetic Bearings MAG’97, Alexandria, USA, pp. 15-24.

Satoru, F., Kouya, Y., Shimomachi, T., Mizumachi, Y., and Kuga M., 1991, “Dynamics of Active Magnetic Thrust Bearings,” JSME International Journal, Series III, 34(3), pp. 404-410.

APPENDIX A

CALIBRATION OF LOAD CELL

Specifications

Excitation :	10VDC
Capacity range:	0-1000 lbs
Accuracy :	± 0.5 % F.S
Repeatability :	± 0.10 % F.S
Temperature range :	60 to 160 ^{0}F
Calibration factor:	3.1403 mv/V

Wiring code :

Red (+)Excitation

Black (-)Excitation

Green (+)Signal

White (-)Signal

Connections

Green (+) and White (-) to voltmeter

Red (+) and Black (-) to power supply

APPENDIX B

2D DRAWINGS OF PARTS OF UHTTMB

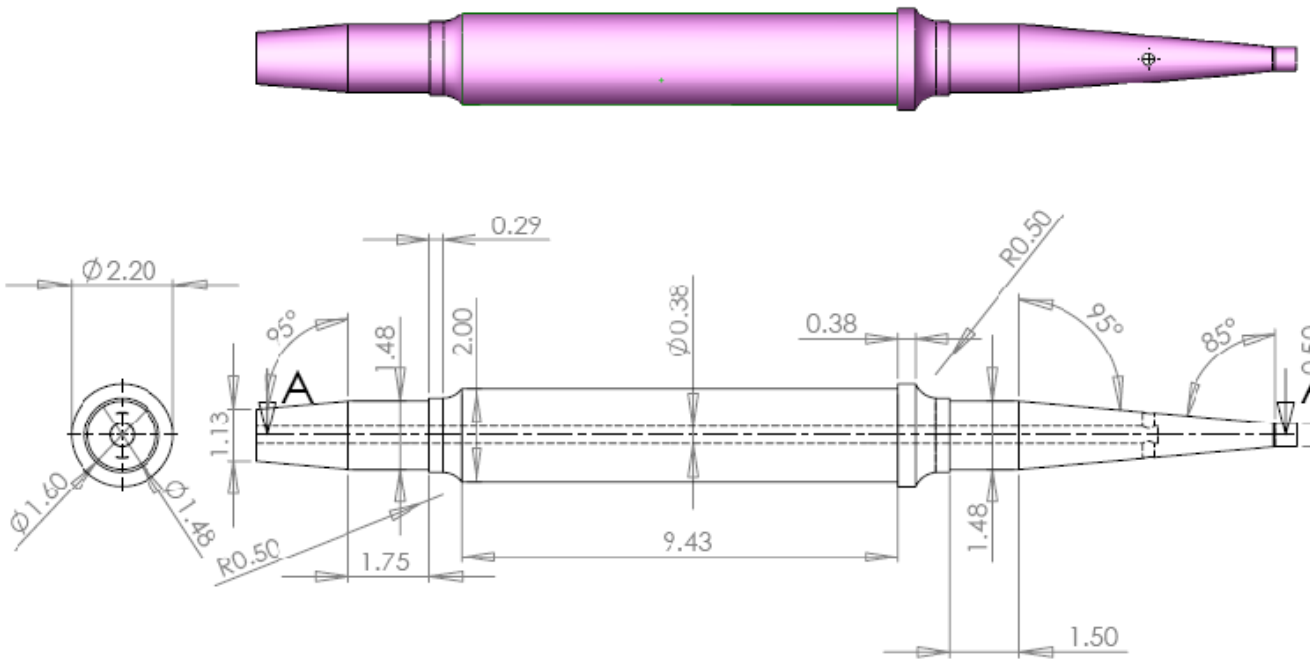

		UNLESS OTHERWISE SPECIFIED:		NAME	DATE
		DIMENSIONS ARE IN INCHES	DRAWN		
		TOLERANCES: FRACTIONAL ± ANGULAR: MACH ± BEND ± TWO PLACE DECIMAL ± THREE PLACE DECIMAL ±	CHECKED		
			ENG APPR.		
			MFG APPR.		
		INTERPRET GEOMETRIC TOLERANCING PER:	Q.A.		
		MATERIAL	COMMENTS:		
		FINISH			
NEXT ASSY	USED ON				
APPLICATION		DO NOT SCALE DRAWING			

TITLE:

Shaft

SIZE	DWG. NO.	REV
A		

SCALE: 1:10 | WEIGHT: | SHEET 1 OF 1

5 4 3 2 1

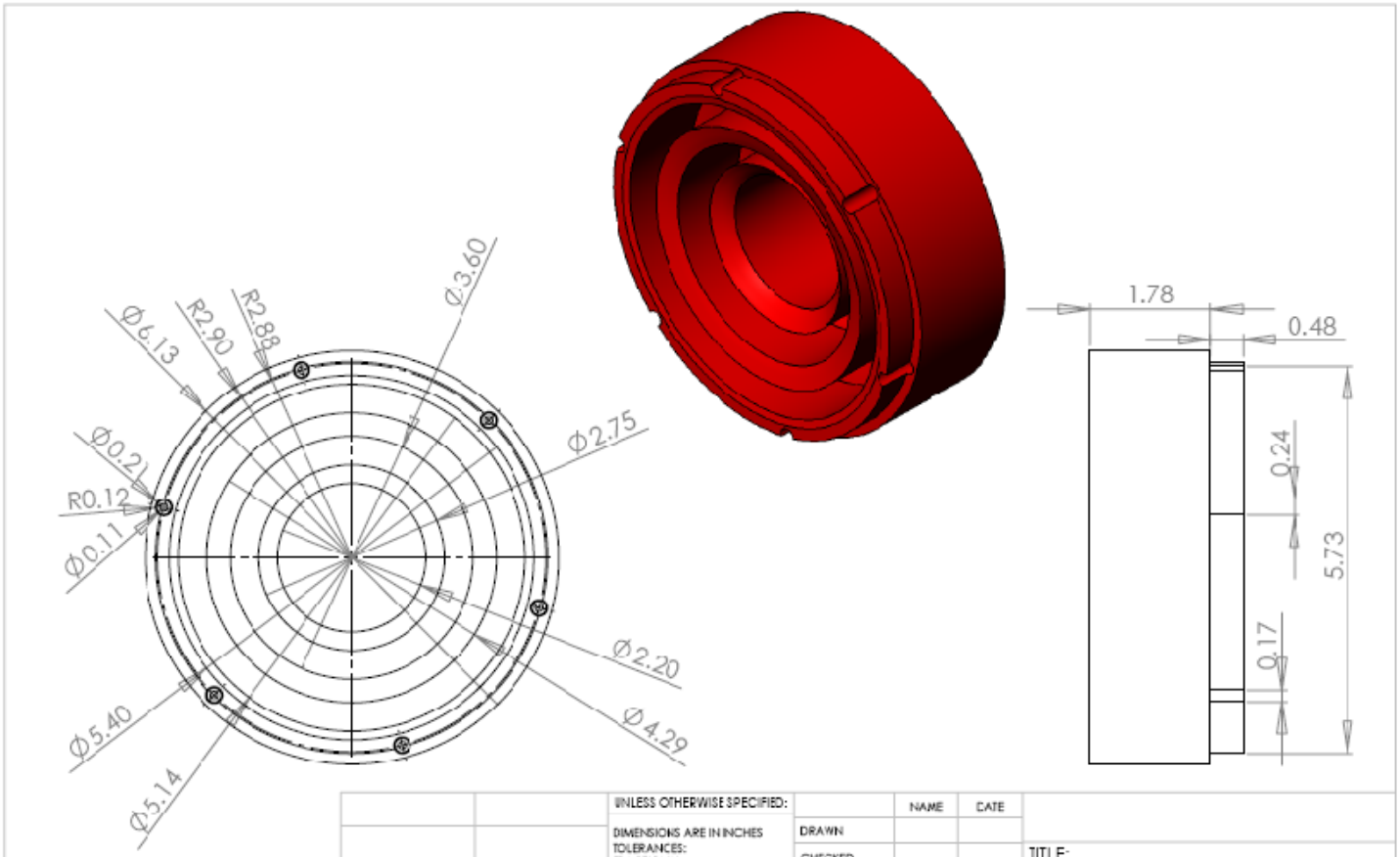

		UNLESS OTHERWISE SPECIFIED:		NAME	DATE
		DIMENSIONS ARE IN INCHES	DRAWN		
		TOLERANCES: FRACTIONAL ±	CHECKED		
		ANGULAR: MACH ± BEND ±	ENG APPR.		
		TWO PLACE DECIMAL ±	MFG APPR.		
		THREE PLACE DECIMAL ±	Q.A.		
		INTERPRET GEOMETRIC TOLERANCING PER:	COMMENTS:		
		MATERIAL			
NEXT ASSY	USED ON	FINISH			
APPLICATION		DO NOT SCALE DRAWING			

TITLE: Stator

SIZE	DWG. NO.	REV
A		
SCALE: 1:5	WEIGHT:	SHEET 1 OF 1

5 4 3 2 1

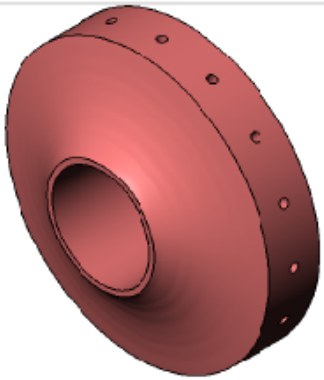

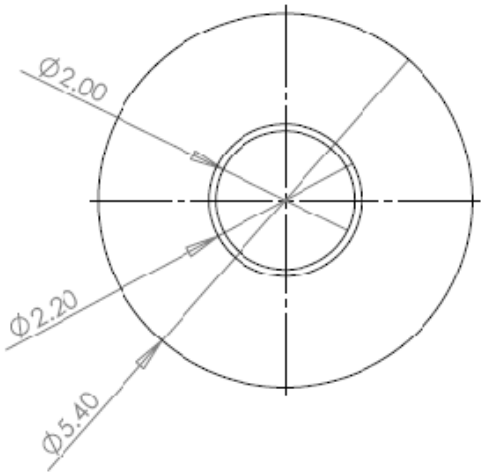

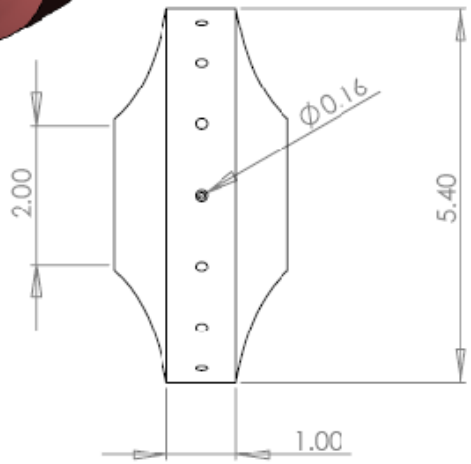

		UNLESS OTHERWISE SPECIFIED:		NAME	DATE
		DIMENSIONS ARE IN INCHES	DRAWN		
		TOLERANCES: FRACTIONAL ±	CHECKED		
		ANGULAR: MACH ± BEND ±	ENG APPR		
		TWO PLACE DECIMAL ±	MFG APPR.		
		THREE PLACE DECIMAL ±	Q.A.		
		INTERPRET GEOMETRIC TOLERANCING PER:	COMMENTS:		
		MATERIAL			
NEXT ASSY	USED ON	FINISH			
APPLICATION		DO NOT SCALE DRAWING			

TITLE:

Rotor

SIZE	DWG. NO.	REV
A		
SCALE: 1:5	WEIGHT:	SHEET 1 OF 1

5 4 3 2 1

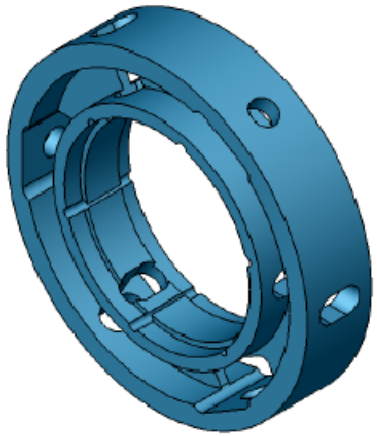

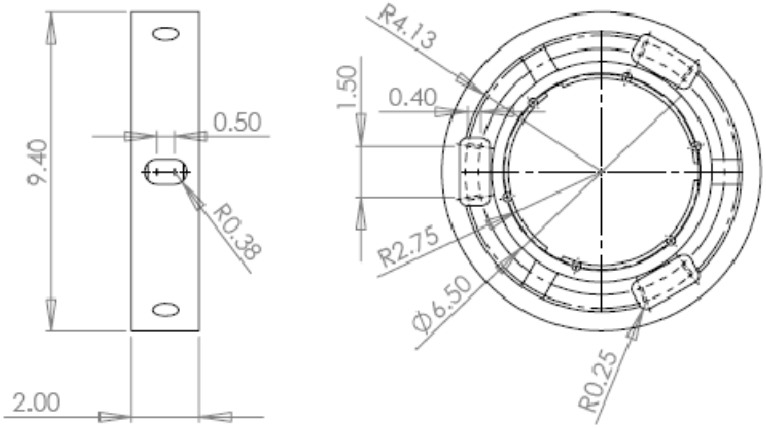

		UNLESS OTHERWISE SPECIFIED:		NAME	DATE
		DIMENSIONS ARE IN INCHES TOLERANCES: FRACTIONAL ± ANGULAR: MACH ± BEND ± TWO PLACE DECIMAL ± THREE PLACE DECIMAL ±	DRAWN		
			CHECKED		
			ENG APPR.		
			MFG APPR.		
		INTERPRET GEOMETRIC TOLERANCING PER:	Q.A.		
		MATERIAL	COMMENTS:		
NEXT ASSY	USED ON	FINISH			
APPLICATION		DO NOT SCALE DRAWING			

TITLE:

stator connector

SIZE	DWG. NO.	REV
A		
SCALE: 1:5	WEIGHT:	SHEET 1 OF 1

5 4 3 2 1

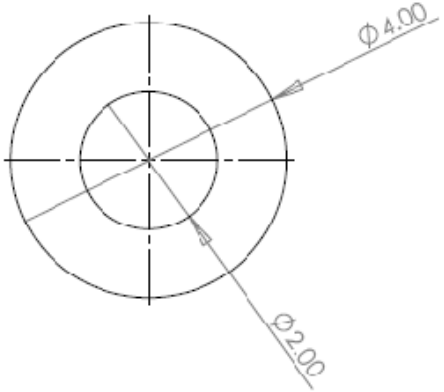

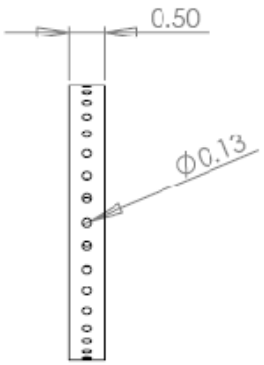

		UNLESS OTHERWISE SPECIFIED:		NAME	DATE
		DIMENSIONS ARE IN INCHES TOLERANCES: FRACTIONAL ± ANGULAR: MACH ± BEND ± TWO PLACE DECIMAL ± THREE PLACE DECIMAL ±	DRAWN		
			CHECKED		
			ENG APPR.		
			MFG APPR.		
		INTERPRET GEOMETRIC TOLERANCING PER:	Q.A.		
		MATERIAL	COMMENTS:		
NEXT ASSY	USED ON	FINISH			
APPLICATION		DO NOT SCALE DRAWING			

TITLE:

Balancing Flywheel

SIZE	DWG. NO.	REV
A		
SCALE: 1:2	WEIGHT:	SHEET 1 OF 1

5 4 3 2 1

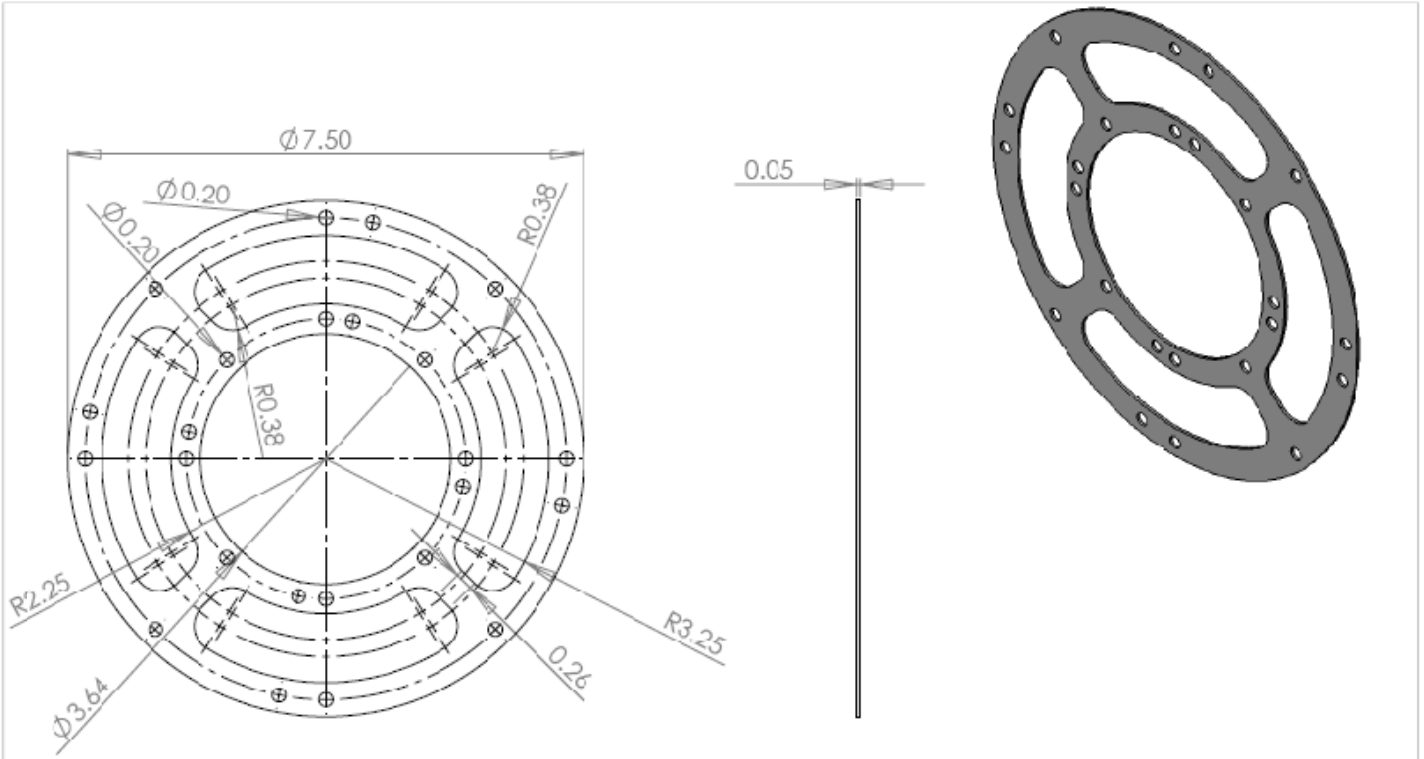

		UNLESS OTHERWISE SPECIFIED:		NAME	DATE
		DIMENSIONS ARE IN INCHES	DRAWN		
		TOLERANCES: FRACTIONAL ± ANGULAR: MACH ± BEND ± TWO PLACE DECIMAL ± THREE PLACE DECIMAL ±	CHECKED		
			ENG APPR.		
			MFG APPR.		
		INTERPRET GEOMETRIC TOLERANCING PER:	Q.A.		
		MATERIAL	COMMENTS:		
NEXT ASSY	USED ON	FINISH			
APPLICATION		DO NOT SCALE DRAWING			

PROPRIETARY AND CONFIDENTIAL

THE INFORMATION CONTAINED IN THIS DRAWING IS THE SOLE PROPERTY OF <INSERT COMPANY NAME HERE>. ANY REPRODUCTION IN PART OR AS A WHOLE WITHOUT THE WRITTEN PERMISSION OF <INSERT COMPANY NAME HERE> IS PROHIBITED.

TITLE: Web

SIZE	DWG. NO.	REV
A		

SCALE: 1:5 WEIGHT: SHEET 1 OF 1

5 4 3 2 1

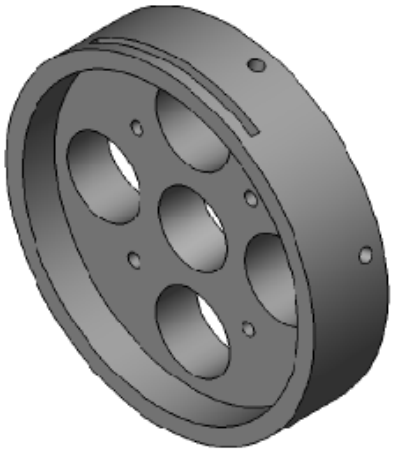

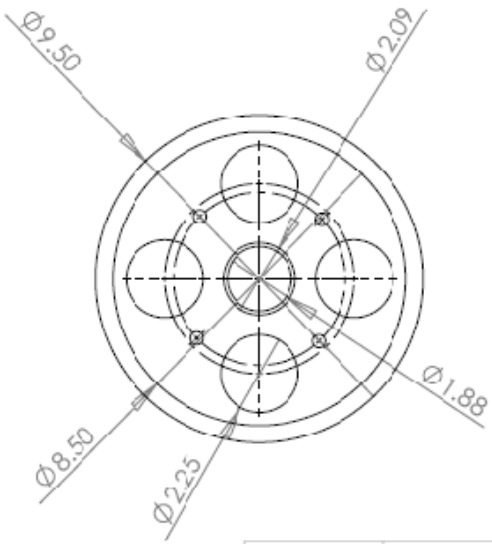

		UNLESS OTHERWISE SPECIFIED		NAME	DATE
		DIMENSIONS ARE IN INCHES TOLERANCES: FRACTIONAL ± ANGULAR: MACH ± BEND ± TWO PLACE DECIMAL ± THREE PLACE DECIMAL ±	DRAWN		
			CHECKED		
			ENG APPR.		
			MFG APPR.		
		INTERPRET GEOMETRIC TOLERANCING PER:	Q.A.		
		MATERIAL	COMMENTS:		
NEXT ASSY	USED ON	FINISH			
APPLICATION		DO NOT SCALE DRAWING			

TITLE:

End cap

SIZE	DWG. NO.	REV
A		
SCALE 1:5	WEIGHT:	SHEET 1 OF 1

5 4 3 2 1

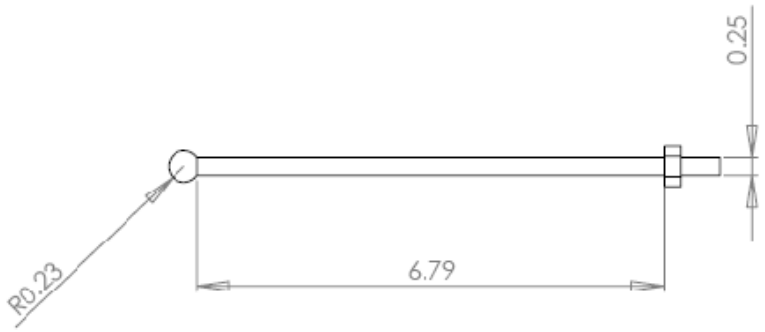

		UNLESS OTHERWISE SPECIFIED:		NAME	DATE
		DIMENSIONS ARE IN INCHES TOLERANCES: FRACTIONAL ± ANGULAR: MACH ± BEND ± TWO PLACE DECIMAL ± THREE PLACE DECIMAL ±	DRAWN		
			CHECKED		
			ENG APPR.		
			MFG APPR.		
		INTERPRET GEOMETRIC TOLERANCING PER	Q.A.		
		MATERIAL	COMMENTS:		
NEXT ASSY	USED ON	FINISH			
APPLICATION		DO NOT SCALE DRAWING			

TITLE:

Tension rod & Nut

SIZE	DWG. NO.	REV
A		
SCALE: 1:5	WEIGH :	SHEET 1 OF 1

5 4 3 2 1

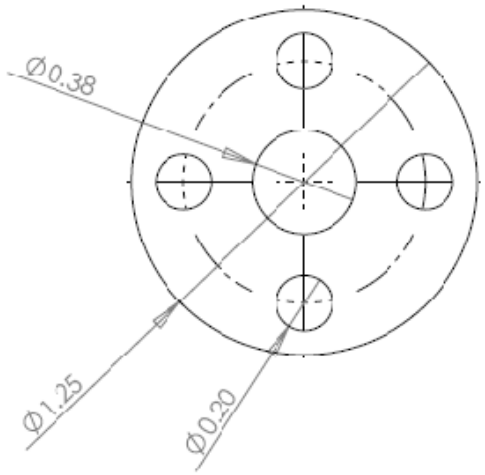

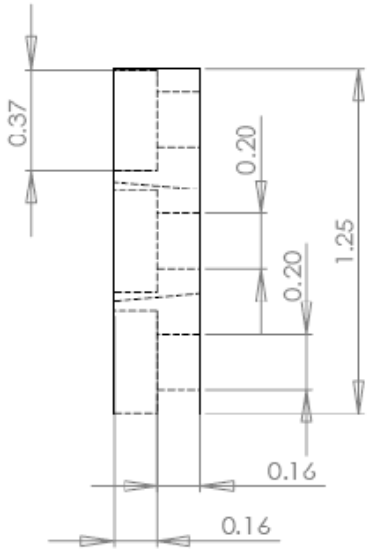

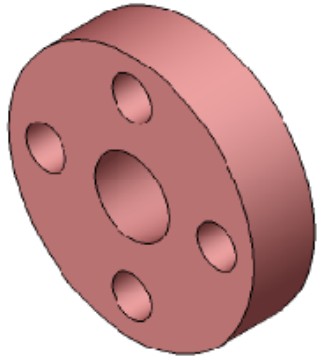

		UNLESS OTHERWISE SPECIFIED:		NAME	DATE
		DIMENSIONS ARE IN INCHES	DRAWN		
		TOLERANCES: FRACTIONAL ±	CHECKED		
		ANGULAR: MACH ± BEND ±	ENG APPR.		
		TWO PLACE DECIMAL :	MFG APPR.		
		THREE PLACE DECIMAL ±	Q.A.		
		INTERPRET GEOMETRIC TOLERANCING PER:	COMMENTS:		
		MATERIAL			
NEXT ASSY	USED ON	FINISH			
APPLICATION		DO NOT SCALE DRAWING			

TITLE: Cap flange for swivel

SIZE	DWG. NO.	REV
A		

SCALE: 1:1	WEIGHT:	SHEET 1 OF 1

5 4 3 2 1

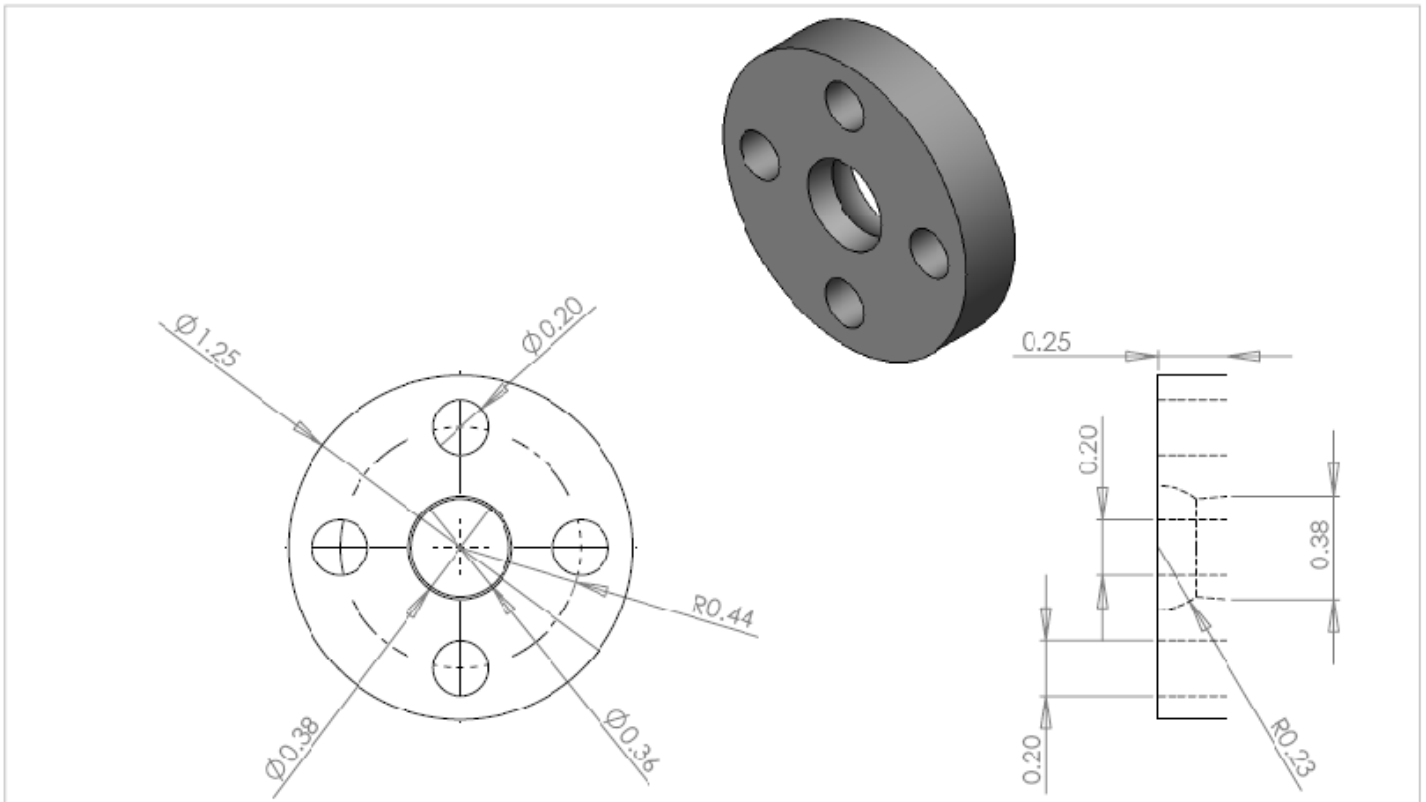

		UNLESS OTHERWISE SPECIFIED:		NAME	DATE
		DIMENSIONS ARE IN INCHES TOLERANCES: FRACTIONAL ± ANGULAR: MACH ± BEND ± TWO PLACE DECIMAL ± THRIE PLACE DECIMAL ±	DRAWN		
			CHECKED		
			ENG APPR.		
			MFG APPR.		
		INTERPRET GEOMETRIC TOLERANCING PER:	Q.A.		
		MATERIAL	COMMENTS:		
NEXT ASSY	USED ON	FINISH			
APPLICATION		DO NOT SCALE DRAWING			

TITLE:

Titanium heat stop foot socket

SIZE	DWG. NO.	REV
A		
SCALE: 1:1	WEIGHT:	SHEET 1 OF 1

5 4 3 2 1

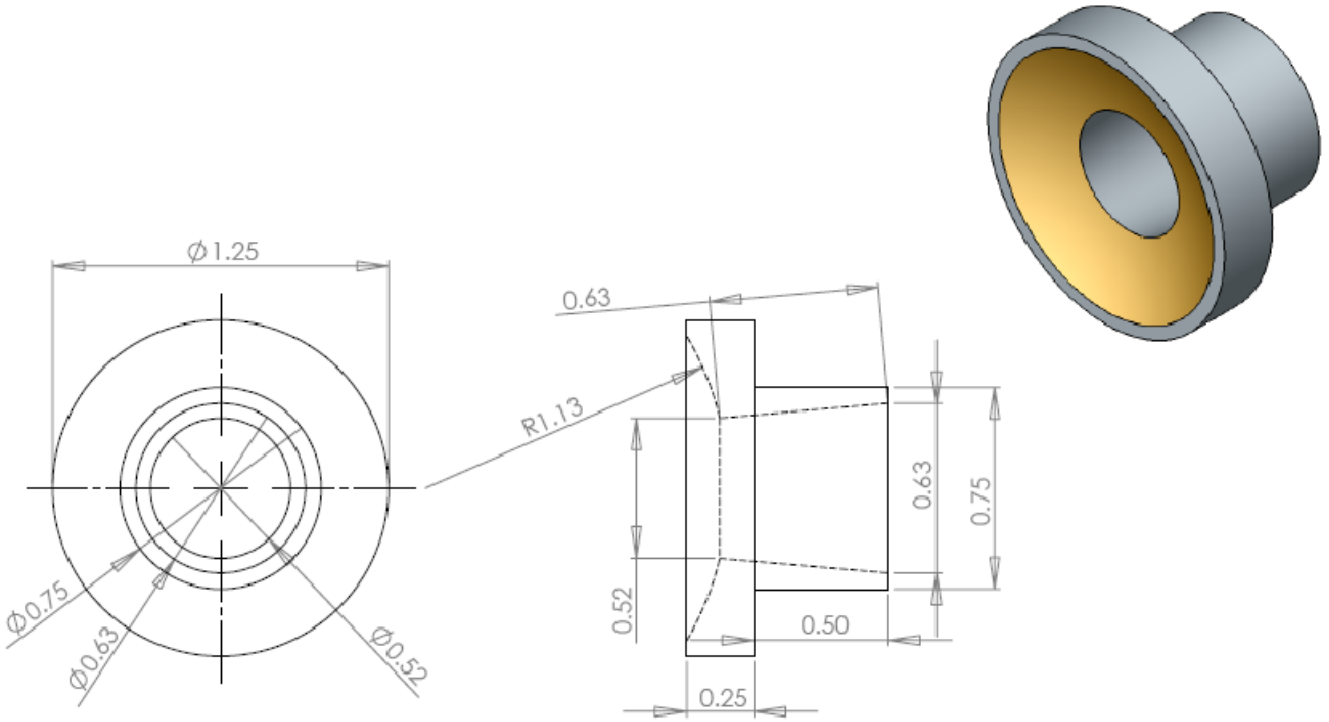

		UNLESS OTHERWISE SPECIFIED:		NAME	DATE
		DIMENSIONS ARE IN INCHES TOLERANCES: FRACTIONAL ± ANGULAR: MACH ± BEND ± TWO PLACE DECIMAL ± THREE PLACE DECIMAL ±	DRAWN		
			CHECKED		
			ENG APPR.		
			MFG APPR.		
		INTERPRET GEOMETRIC TOLERANCING PER:	Q.A.		
		MATERIAL	COMMENTS:		
NEXT ASSY	USED ON	FINISH			
APPLICATION		DO NOT SCALE DRAWING			

TITLE: Macor standoff stator connector

SIZE	DWG. NO.	REV
A		
SCALE: 2:1	WEIGHT:	SHEET 1 OF 1

5 4 3 2 1

VITA

Name: Desireddy Vijesh Reddy

Address: Texas A&M University,
Department of Mechanical Engineering,
3123 TAMU,
College Station, TX 77843-3123.

Email Address: vijeshreddy@tamu.edu

Education: B.E., Mechanical Engineering, Jawaharlal Nehru Technological University, India, 2006